ChemComm

ROYAL SOCIETY OF CHEMISTRY

FEATURE ARTICLE

View Article Online
View Journal

Cite this: DOI: 10.1039/d4cc04388j

Aromatic foldamer-derived transmembrane transporters

Danyang Zhang, Wenju Chang,* Jie Shen * and Huaqiang Zeng *

This review is the first to focus on transmembrane transporters derived from aromatic foldamers, with most studies reported over the past decade. These foldamers have made significant strides in mimicking the essential functions of natural ion channel proteins. With their aromatic backbones rigidified by intramolecular hydrogen bonds or differential repulsive forces, this innovative family of molecules stands out for its structural diversity and functional adaptability. They achieve efficient and selective ion and molecule transport across lipid bilayers *via* carefully designed helical structures and tunable large cavities. Recent developments in this field highlight the transformative potential of foldamers in therapeutic applications and biomaterial engineering. Key advances include innovative molecular engineering strategies that enable highly selective ion transport by fine-tuning structural and functional attributes. Specific modifications to macrocyclic or helical foldamer structures have allowed precise control over ion selectivity and transport efficiency, with notable selectivity for K^+, Li^+, H^+ and water molecules. Although challenges remain, future directions may focus on more innovative molecular designs, optimizing synthetic methods, improving membrane transport properties, integrating responsive designs that adapt to environmental stimuli, and fostering interdisciplinary collaborations. By emphasizing the pivotal role of aromatic foldamers in modern chemistry, this review aims to inspire further development, offering new molecular toolboxes and strategies to address technological and biological challenges in chemistry, biology, medicine, and materials science.

Received 27th August 2024,
Accepted 17th October 2024

DOI: 10.1039/d4cc04388j

rsc.li/chemcomm

1. Introduction

At the core of cell biology, transmembrane ion transporters play a crucial role. These channel proteins, located on cell membranes, finely regulate the flow of ions inside and outside cells to maintain internal environment stability and participate in key biological processes such as nerve conduction, muscle contraction, and cell signaling. A deep understanding of these transporters encompasses research on naturally occurring ion channels as well as the development and optimization of artificially synthesized transporters. With the rapid advancement of biotechnology, particularly in protein engineering and structural biology, our understanding of channel proteins has reached unprecedented depths.

College of Chemistry Fuzhou University Fuzhou, Fujian 350116, China.
E-mail: wenjuchang@fzu.edu.cn, shenjie@fzu.edu.cn, hqzeng@fzu.edu.cn

Danyang Zhang

Danyang Zhang obtained her BSc in Pharmacy in 2022 from Hebei Normal University, China. In the same year, she was admitted to the College of Chemistry at Fuzhou University to pursue her MSc research under the supervision of Professor Huaqiang Zeng. Her research focuses on the structural and functional analysis of self-assembled structures through computational methods.

Wenju Chang

Wenju Chang received his PhD in chemistry from Nanjing University under the supervision of Professor Yong Liang in 2019. From 2019 to 2023, he worked as an associate researcher at the School of Chemistry and Chemical Engineering, Nanjing University. In 2023, he joined Fuzhou University as a lecturer, where his research interests focus on organic synthesis, novel biomimetic artificial channels, and DFT calculations.

In the early 20th century, scientists began to recognize the ion permeability of cell membranes[1,2] and observed significant differences in ion concentrations between inside and outside cells, laying the foundation for modern research on transmembrane ion transporters. Modern research techniques, including X-ray crystallography,[3] nuclear magnetic resonance (NMR) imaging,[3] and computational simulations, have equipped scientists with powerful tools to precisely unravel the three-dimensional structures of these complex proteins and explore their detailed ion transport and gating mechanisms.

The discovery of potassium,[4,5] sodium,[6,7] calcium[8,9] and chloride[10] ion channels—protein channels on cell membranes that selectively allow specific ions to pass—marked a breakthrough in understanding the ion regulation mechanism (Fig. 1). And the discovery of various ion pumps, such as the sodium–potassium pump[11] and calcium pumps,[12] further propelled the development of this field. These pumps transport ions against concentration gradients by consuming energy and are crucial for maintaining ion balance in cells. These progresses have not only deepened our understanding of the functions of channel proteins but also provided innovative avenues for the development of new drugs and the treatment of channels associated diseases.

The inspiration for the design of artificial transporters often originates from natural systems, aiming to mimic or even surpass the functionalities of natural ion channels. Therefore, delving into the natural transmembrane ion transporters, research on artificially synthesized transporters has also been continuously advancing. In the late 1960s, the discovery of crown ethers[13] opened up a brand new scientific research fore-frontier involving the synthesis of such molecules and their ion-complexing properties. Concurrently, the discovery of natural ion carriers like valinomycin[14] has sparked interests in the study of amphiphilic macrocyclic compounds to mimic membrane transport mechanisms. In 1982, Tabushi introduced a novel artificial channel derived from A,B,D,F-tetrasubstituted β-cyclodextrin, which achieved highly efficient and fast Co^{2+} ion transport through its amphiphilic structure and multiple metal ion binding sites across the membrane. Notably, its transport rate for Co^{2+} (4.5×10^{-4} s^{-1} at 55 μM) significantly surpasses those of traditional carriers (Fig. 2(a)).[15] In 1990, Gokel *et al.* reported the design of hydraphiles, utilizing crown ethers as ion-selective headgroups and polar center elements to form single-molecule channels selectively mediating the transport of sodium (Na^+) and potassium ions (K^+), which could be blocked by silver ions (Ag^+) (Fig. 2(b)).[16] In 1994, Ghadiri, Granja, and Buehler demonstrated the ability of self-assembling cyclic peptides to serve as artificial transmembrane ion channels (Fig. 2(c) and (d)).[17,18] Early studies by Matile group focused on creating artificial β-barrels by using rigid-rod scaffolds as privileged staves for transporting ions and small molecules (Fig. 2(e)).[19,20] In 2020, Matile applied this type of synthetic supramolecular pores to sense changes in enzymatic activity through the reversible blocking by substrates or products. This approach enables high-throughput and "naked-eye" detection of various enzymatic reactions, characterized by high sensitivity, strong adaptability, and ease of operation (Fig. 2(f) and (g)).[21] Entering the 21st century, the rapid development of supramolecular chemistry provides new avenues for designing novel ion transporters. By utilizing non-covalent interactions such as H-bonding, hydrophobic effects, and ion–dipole interactions, coupled with self-assembly techniques, selective binding and transport of specific ions on membranes can be achieved. Anion transporters[22–29] can effectively transport chloride ions, bicarbonate ions, *etc.*, showing potential therapeutic applications in cell experiments. Cation transporters can efficiently transport protons, potassium ions, ammonium ions, *etc.*, demonstrating potential prospects in certain disease treatments.[30–34] Additionally, the rapid development of artificial water channels endows them with high salinity water exclusion functions, bringing enormous potential in areas like seawater desalination and wastewater recycling.[35–40]

Jie Shen

*Jie Shen received his PhD in chemistry from National University of Singapore under the guidance of Professor Huaqiang Zeng in 2014. From 2015 to 2021, he carried out postdoctoral research work at the Institute of Bioengineering and Nanotechnology and then at NanoBio Lab, A*STAR. He joined the Fuzhou University as a Professor in 2022, with research interests focusing on creating novel biomimetic artificial channels using H-bonded aromatic foldamers for their interdisciplinary applications across chemistry, material sciences and medicine.*

Huaqiang Zeng

*Huaqiang Zeng received his BSc from University of Science and Technology of China in 1996 and PhD from University at Buffalo in 2002 under the supervision of Prof. Bing Gong. From 2006 to 2014, he worked as an Assistant Professor at NUS. After working as Team Leader and Principal Research Scientist from 2014 to 2020 at A*STAR, he joined Northwestern Polytechnical University as a Professor in 2020 and moved to Fuzhou University in 2022, with a passion to create biomimetic artificial channels for their interdisciplinary applications across chemistry, material sciences, and medicine.*

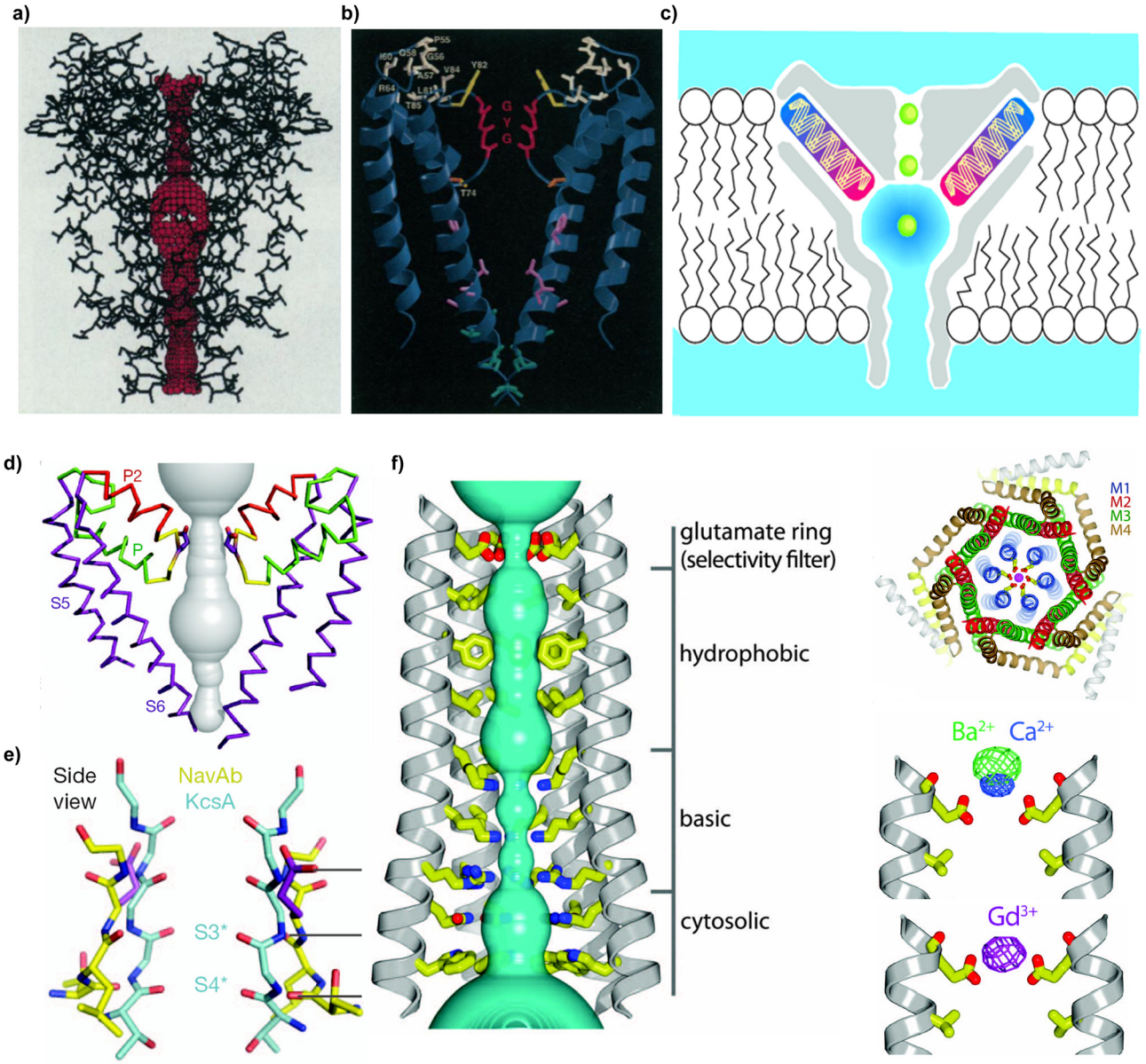

Fig. 1 The crystal structure of (a) and (b) potassium channel KcsA, (d) nad (e) sodium channel NavAb and (f)–(h) calcium channel. (a) Within a stick model of the channel structure is a three-dimensional representation of the minimum radial distance from the center of the channel pore to the nearest van der Waals protein contact. (b) Selectivity filter that dictates the highly selective transport of K^+ ions. (c) Mechanism by which the K^+ channel stabilizes a cation in the middle of the membrane, involving a large aqueous cavity that stabilizes an ion (green) in the otherwise hydrophobic membrane interior and oriented helices that point their partial negative charge (carboxyl end, red) towards the cavity where a cation is located. (d) Architecture of the NavAb pore with its pore volume shown in grey. (e) Superposition of NavAb and the KcsA selectivity filters, which achieve ion selectivity through size matching of hydrated ions and dehydration energy, respectively. (f) View of the pore of the calcium channel. Within a ribbon representation of four M1 helices (two in the foreground were removed for clarity) is a representation (teal color) of the minimal radial distance from the center to the nearest van der Waals contact. (g) An orthogonal view of the channel from the extracellular side, with a cation binding in the external site. (h) Ba^{2+} and Ca^{2+} binding as well as Gd^{3+} binding sites. Reproduced with permission from ref. 4 (Copyright 1998 The American Association for the Advancement of Science), ref. 7 (Copyright 2011 Springer Nature) and ref. 9 (Copyright 2012 The American Association for the Advancement of Science).

These artificial transporters not only hold significance in basic research but also exhibit immense potential in applications such as drug delivery, molecular machines, and sensors.

Foldamer was coined by American chemist Samuel H. Gellman in the 1990s to describe any molecule, having strong tendency to adopt specific compact conformations by virtue of non-covalent forces.[41] These molecules can spontaneously generate regular secondary structures, stabilized by intra- and intermolecular non-covalent interactions such as H-bonds, π–π interactions, and hydrophobic interactions, among others. Nevertheless, such a concept can be traced back to the 1960s when scientists began exploring the synthesis and structure of

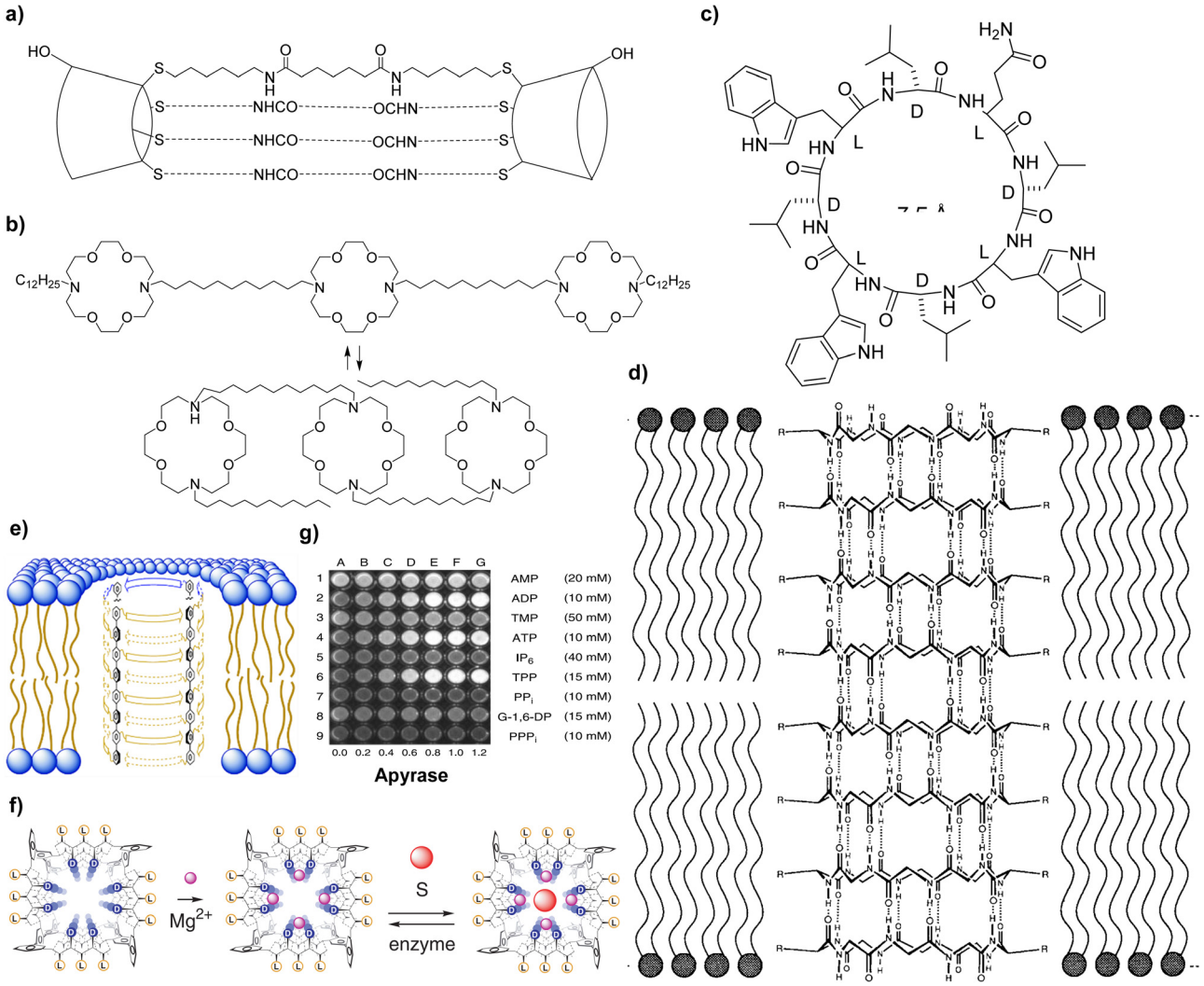

Fig. 2 Representative earlier efforts toward constructing artificial ion channels. (a) The first artificial Co^{2+}-transporting ion channel. (b) Chemical structure of tris(macrocycle) hydraphiles as unimolecular ion channel. (c) A representative macrocyclic structure composed of alternative D and L amino acid residues, which self-assembles into tubular configuration emphasizing the antiparallel stacking *via* the extensive network of intermolecular hydrogen-bonding interactions as shown in (d). (e) Rigid-rod β barrels that are active for ion transport in lipid bilayers. (f) Pore **1** as enzyme activity detector. Changes in the obstruction of dye efflux from liposomes through host $1\supset Mg^{2+}n$ by either substrate **S** or product due to substrate conversion are reported by changes in dye fluorescence. (g) End-point substrate screening using $1\supset Mg^{2+}n$. Substrate candidates at $c > K_D$ (lanes 1–9) were incubated for 20 hours with increasing apyrase concentrations (lanes A– G). The LUVs⊃CF and 1 were then added, and fluorescence was measured within ≲30 min. Increasing CF emission with increasing enzyme concentration correctly identified ADP, ATP, and TPP (lanes 2, 4, 6, respectively) as substrates. Reproduced with permission from ref. 15 (Copyright 1982 Elsevier), ref. 16 (Copyright 1990 The American Chemical Society), ref. 18 (Copyright 1994 Springer Nature) and ref. 21 (Copyright 2002 The American Association for the Advancement of Science).

non-natural peptide-like compounds. For example, homopolymers composed of β-amino acids, known as members of the nylon-3 family, were investigated.[42,43] Among them, poly(β-isobutyl-L-aspartate) is one of the earlier polymers that has been intensively studied, with various proposed structures including 14-helix and 18-helix structures.[44–48]

Over the past few decades, scientists have explored various non-natural oligomers, expanding foldamer research to multiple structural types. Depending on their constituent units, foldamers can be classified into several categories: aliphatic peptide foldamers[49,50] that exhibit secondary structures similar to natural proteins such as α-helices and β-sheets; nucleic acid foldamers capable of forming structures similar to DNA and RNA such as G-quadruplexes,[51] and aromatic foldamers that are rigidified by non-covalent forces and that generally take crescent-shaped or helical conformations.[41,52,53]

In particular, research in aromatic foldamers began in 1994 when Hamilton and colleagues reported the first batch of aromatic amide-based foldamers (Fig. 3(a) and (e)).[54,55] Subsequent pioneering studies by Lehn (Fig. 3(c) and (d)),[56,57] and Gong (Fig. 3(b))[58,59] laid the solid foundation for aromatic foldamer chemistry, demonstrating the possibility of generating diverse stable secondary structures from their folding codons through intramolecular H-bonds and repulsive forces (Scheme 1).[35,52,53,60–68]

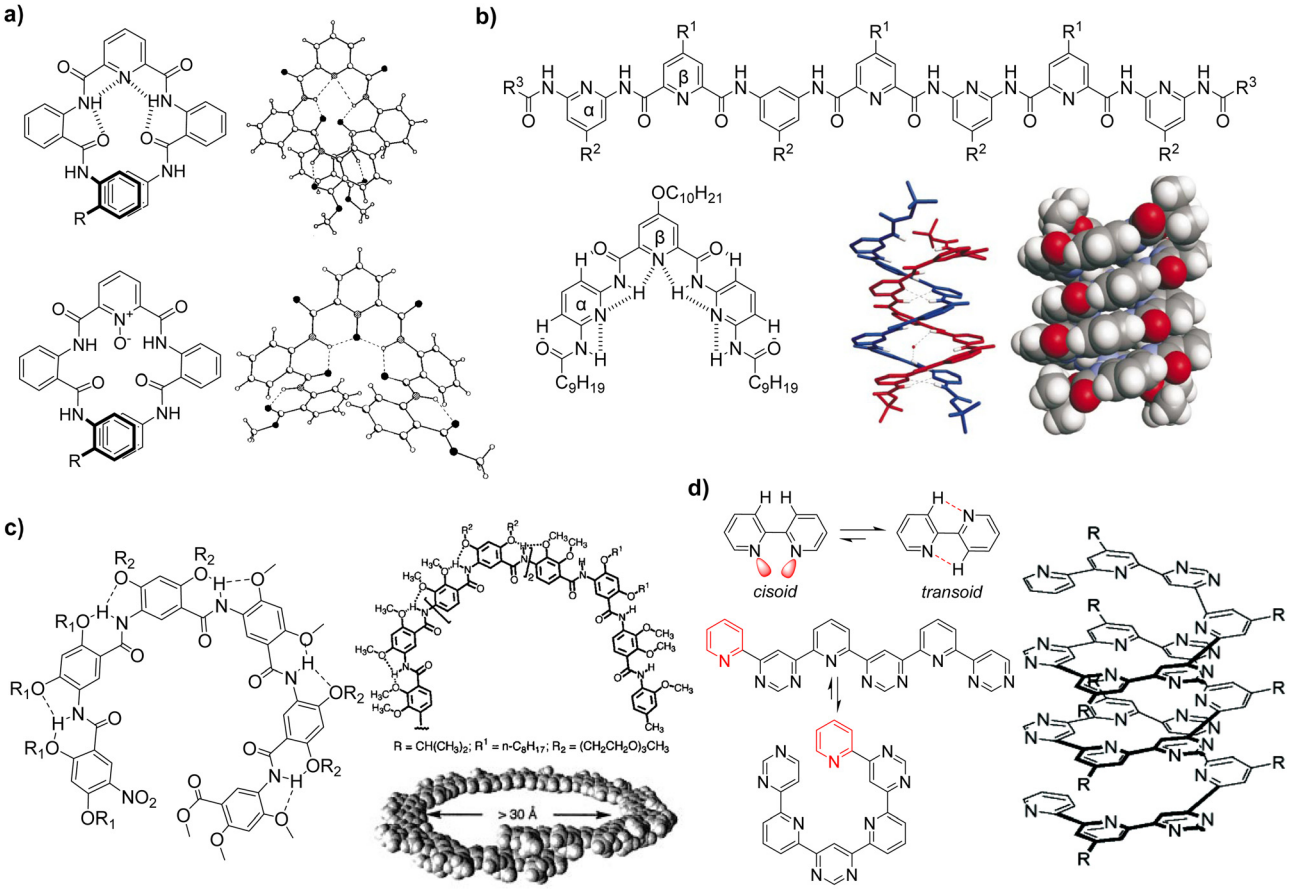

Fig. 3 Pioneering classes of aromatic foldamers. Reproduced with permission from ref. 54 (Copyright 1994 Wiley), ref. 55 (Copyright 1997 The American Association for the Advancement of Science), ref. 56 (Copyright 2000 Springer Nature), ref. 57 (Copyright 1997 Wiley) and ref. 58 (Copyright 2000 The American Chemical Society).

Aromatic foldamers have gained widespread attention in recent years due to their chemical stability, structural diversity and predictability as well as high functional tunability (Scheme 1).[35,52,53,60–68] Within the context of lipid membrane, by designing specific structures and functional groups, the cavity size and functions of the channels may be optimized to achieve selective recognition and transport of specific ions[69,70] and their rigidity and stability may contribute to the formation of stable channel structures, thereby enhancing ion transport efficiency.

Indeed, recent advances along this line have confirmed the great advantages in using aromatic foldamers for constructing powerful functionally diversified transmembrane transporters, which are the focus of this review. We will review key scientific findings in this area, followed by outlining the existing challenges, potential research directions and functional applications in the future.

2. H-bonded macrocyclic foldamers as ion transporters

In 2008, Gong *et al.* reported highly conductive transmembrane ion channels built from aromatic oligoamide macrocycles (Fig. 4).[71] These macrocyclic molecules were synthesized through a one-pot condensation reaction from corresponding diamines and diacid chlorides,[72,73] with backbone folding induced by three-center intramolecular H-bonds. They possess a relatively flat aromatic backbone and a large aromatic surface area, facilitating their self-assembly into nanotubular structures through face-to-face stacking. This generates transmembrane channels that possess an internal hydrophilic cavity of about 8.5 Å in diameter. Using ^{23}Na NMR spectroscopy to measure the concentration-dependent Na^+ ion exchanges, the Na^+ transport rate constant for macrocycle **1d** was determined to be approximately 5.65 s^{-1}, a transport rate that is nearly half that of gramicidin A (gA). Additionally, **1b** exhibits a conductivity similar to that of **1a**, suggesting that variations in side chain do not noticeably affect the ion conduction properties of the channels. Rather, it is the macrocyclic backbone that defines the channel's diameter and conductivity.

In their subsequent study in 2015, Gong *et al.* found that the **1**-like macrocyclic backbone with slightly reduced constraint by changing two three-center H-bonds to two-center H-bonds while introducing an amide group around the macrocyclic exterior exhibits extremely strong stacking among macrocycles.[74] Inspired by this, the research team removed

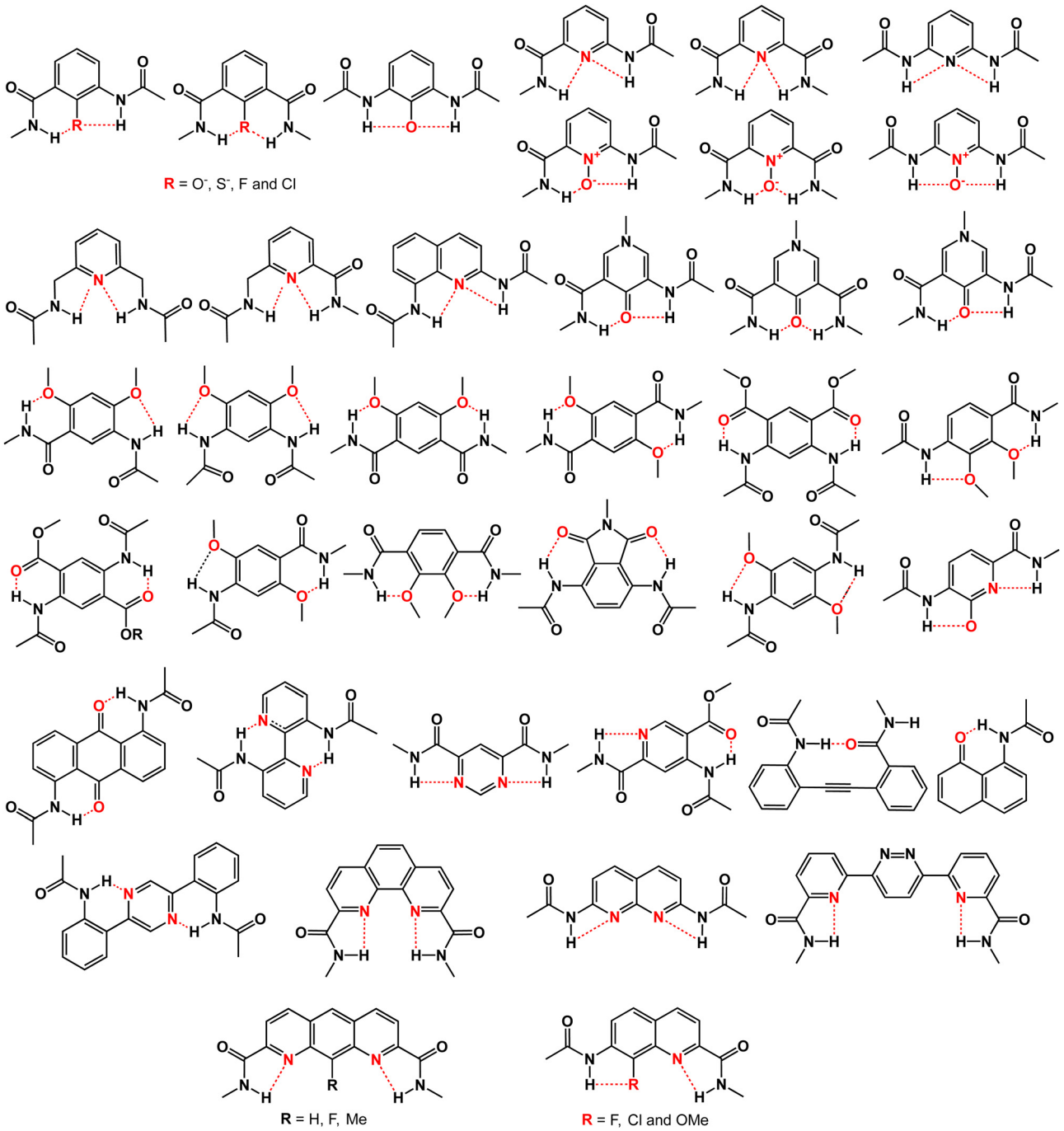

Scheme 1 Aromatic folding codons for constructing diverse types of H-bonded aromatic foldamers.

two three-center H-bonds by replacing one of the dicarboxyl building block with a amide-substituted diethynylbenzene unit, generating macrocycles **2** (Fig. 5).[75] This hybrid backbone design not only maintains the macrocyclic nature but also allows for various functional groups to be introduced into the internal cavity, significantly altering ion transport behavior. In lipid bilayer experiments, nanopores functionalized with fluorine or hydrogen atoms (**2a** and **2b**) demonstrate significant proton transport capabilities, albeit to different extents. Containing an amino group, **2c** facilitates the transport of chloride ions while rejecting protons. This is because the amide group on the *ortho* position additionally reduces the electron density of the amino H-atoms, making it more partially positively charged. This leads to the transport of Cl^- and rejection of protons. In contrast, the methyl group in **2d**, being smaller and hydrophobic, shows weaker proton repulsion and less attraction to Cl^- compared to **2c**. These differences in ion transport property arise from functional group-dependent electrostatic potentials within the pore. A highlight of this study is the precise design and adjustment of functional groups within the

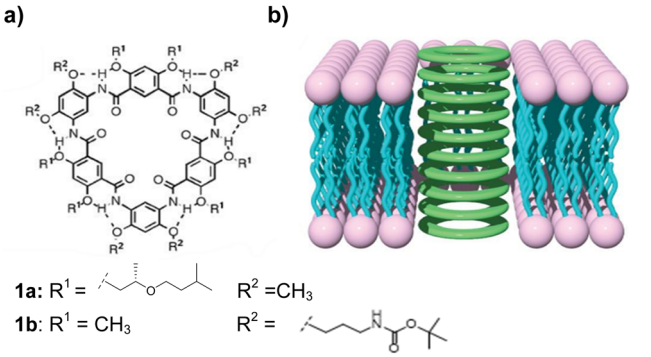

Fig. 4 (a) Shape-persistent macrocycles **1**. (b) Schematic diagram of transmembrane transport in a lipid bilayer. Reproduced with permission from ref. 71 (Copyright 2008 The American Chemical Society).

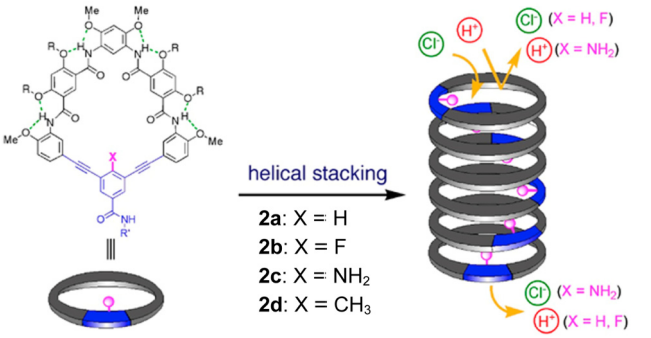

Fig. 5 Schematic diagram of transmembrane transport of macrocycles **2**. Reproduced with permission from ref. 75 (Copyright 2016 The American Chemical Society).

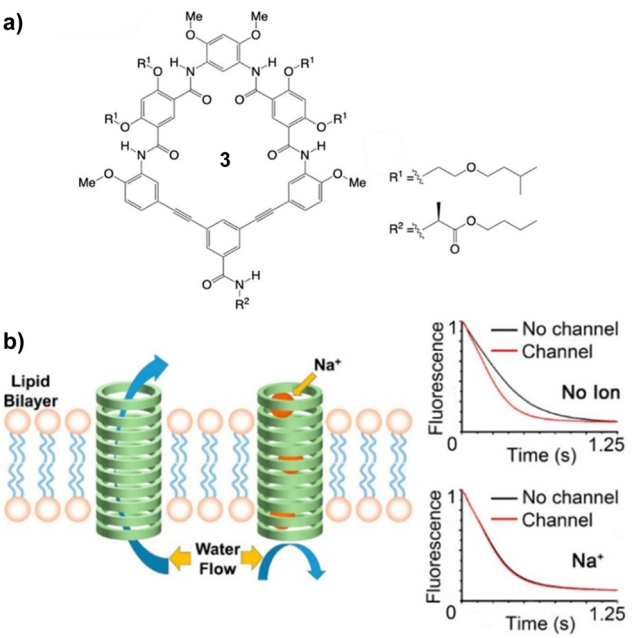

Fig. 6 (a) Structural representation of macrocycles **3**. (b) Schematic diagrams of transmembrane water transport under conditions with and without cations. Reproduced with permission from ref. 76 (Copyright 2021 The American Chemical Society).

internal cavity of the macrocyclic compounds, offering new possibilities for developing synthetic channels and devices with specific selectivities and specificities.

The same group extended the above work by further removing the internal functional groups **X**, generating macrocycles **3** (Fig. 6). This minor alteration in structure results in a new type of hydrophobic–hydrophilic mixed lumen and consequently drastic changes in transport performance. Approaching the functional characteristics of biological aquaporins, nanotubes formed from self-assembled **3** achieve precise control over water transport.[76] By altering the concentration of alkali metal ions inside the nanopore, the flow rate of water molecules can be regulated. That is, Na^+ ions significantly reduce the water transport rate with Li^+, K^+ and Cs^+ ions having a lesser impact. The uniqueness of this nanopore apprently lies in its internal hydrophilic part, which provides binding sites for metal ions that significantly affect the flow of water molecules. Molecular dynamics (MD) simulations further reveal how the strength of the interaction between ions and the hydrophilic parts, as well as the interaction of ions with the first shell of water molecules within the pore, regulate the water transport rate. Therefore, the design and synthesis method of this nanopore provides a flexible platform that allows researchers to systematically explore various factors affecting water transport by introducing different metal ion binding sites.

In 2017, Xin *et al.* reported a novel type of functional hydrazide macrocyclic ion channel **4** with unique pH sensitivity, demonstrating different K^+/Cl^- selectivities in buffer solutions of varying pH values (Fig. 7).[77] Supported by the phenylalanine-derived tripeptide chains that enhance the aromatic framework's membrane embedding capability, macrocyclic **4** incorporates three inward-facing amine groups, which confer pH responsiveness to the channel. Experimental results show that **4** effectively mediates transmembrane ion transport, especially with significant changes in ion selectivity in response to pH shifts. Under alkaline conditions at pH 10.0, macrocycle **4** predominantly transports K^+, while at an acidic pH of 4.0, the transport activity for K^+ significantly decreases, and that for Cl^- increases. This pH-dependent ion selectivity change is primarily due to alterations in the protonation and deprotonation states of amines and carboxyl groups in the channel, which in turn changes the internal and external charge distributions of the channel. Moreover, experiments conducted on planar lipid bilayers using the planar lipid bilayer workstation further confirm that **4** functions through a channel mechanism. Its conductance (γ) is comparable to that of the highly efficient gA channel, indicating high efficiency in transporting K^+. Overall, this study developed a new class of pH-sensitive ion channels that achieve controlled ion selectivity through simple synthetic steps and responsiveness to environmental pH.

Xin *et al.* continued the inner modification strategy, reporting on a novel pH-sensitive, cation-selective hydrazide macrocyclic channel **5** characterized by having multiple carboxyl

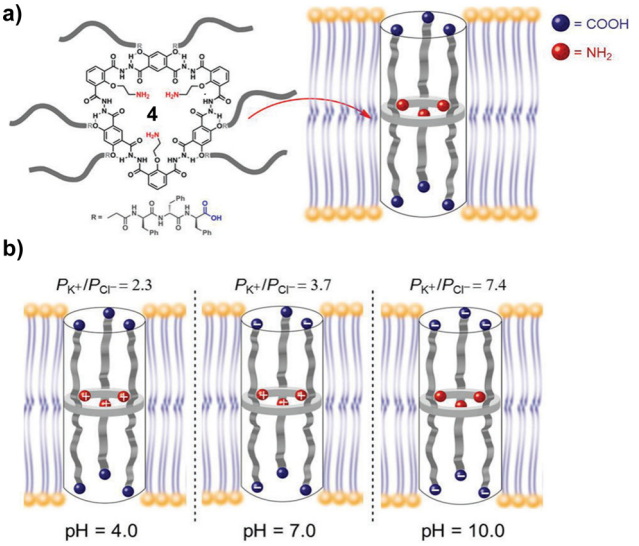

Fig. 7 (a) A schematic diagram for the transmembrane channels formed by **4** in the lipid bilayer. (b) Illustration of charge changes occurring in the macrocyclic channels upon variation of the pH value. Reproduced with permission from ref. 77 (Copyright 2017 The Royal Society of Chemistry).

groups located in its internal cavity (Fig. 8).[78] Channel **5** facilitates highly efficient transmembrane transport of NH_4^+, even surpassing the known gA. This high efficiency is likely due to NH_4^+'s ability to form H-bonds and electrostatic interactions with the carboxyl and carbonyl groups inside the channel, thereby. The pH sensitivity of **5** is one interesting feature: as the electrolyte pH changes, the channel's selectivity for K^+ and Cl^- also changes. Under alkaline conditions, the selectivity for K^+ increases, likely due to the deprotonation of the carboxyl groups in the internal chamber and opening, which generates a negative charge and thereby a strong electrostatic attraction to K^+ ions. Under acidic conditions, the selectivity for K^+ decreases

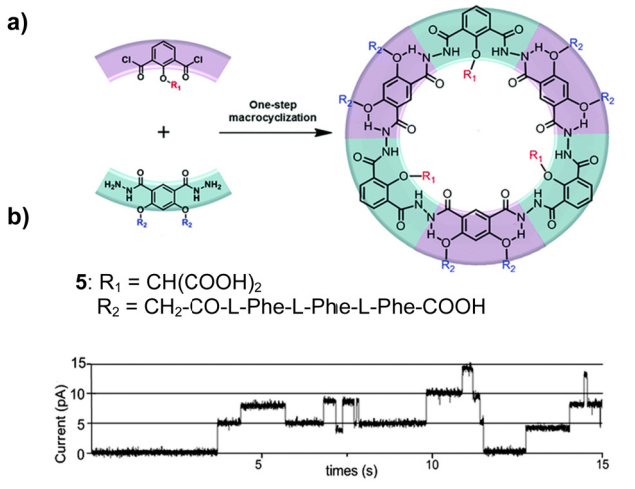

Fig. 8 (a) One-pot synthesis of macrocycle **5** at room temperature. (b) Single channel current traces of **5** (0.5 mM) in the planar lipid bilayer at +100 mV. Both chambers were filled with 1.0 M NH_4Cl. Reproduced with permission from ref. 78 (Copyright 2017 The Royal Society of Chemistry).

because the protonation of the carboxyl groups reduces the negative charge density inside the channel. This pH sensitivity gives these channels potential applications in biosensing and smart material design. The design of the channels also allows for performance tuning by altering the number and position of carboxyl groups, providing flexibility for further molecular engineering. This study not only demonstrates a new type of pH-sensitive ion channel but also provides a new strategy for regulating and optimizing the performance of artificial ion channels.

Madhavan's group designed anion-transporting triamide macrocycles, having amide H-atoms decorating the cavity interior (Fig. 9).[79] These compounds are easy to synthesize and can be manipulated through externally functionalizable pendant groups to enhance membrane permeability.[80] Particularly, cholesterol group serves as an efficient lipid-anchoring group, endowing **6** with low EC_{50} value of 0.44 μM for Cl^- transport through an OH^-/X^- counter-transport mechanism (Fig. 9(a)). They also found that **6** shows high selectivity for SCN^- and Cl^-. This characteristic is likely determined by the H-bonding capability of the anion with the amide NH bonds within the macrocycle. Furthermore, the ion transport activity of **6** is highly sensitive to temperature and membrane rigidity, suggesting that it might function through a carrier mechanism rather than a channel mechanism (Fig. 9(b)). Unlike **6** that may behaves like a carrier, macrocycle **7** transport anions through a channel mechanism (Fig. 9(c) and (d)).[81] Similar to **6**, the NH groups capable of forming H-bonds with anions and electron-deficient aromatic units for binding anions through anion–π interactions within the macrocycle work together to allow **7** to preferentially transport Cl^- with high selectivity against other anions but somewhat low efficiency (EC_{50} value = 29.2 μM).

Building upon their past research experience that backbone of reduced constraints can also form well-folded structures, Gong recently envisioned and demonstrated a novel class of partially rigidified aromatic pentaamide macrocycles (Fig. 10(a)), which exhibit a unique 5-fold-symmetric planar aromatic backbone.[82] Readily prepared through a mild one-pot method, these macrocycles feature two sets of five H-atoms each from amide and benzene functional groups oriented towards the macrocyclic center. These H-atoms define a hydrophobic and electropositive cavity of approximately 4.6 Å after excluding van der Waals radii of two H-atoms, which is well-suited for anion binding. As a result, these macrocycles bind halide anions (Fig. 10(a)), particularly oxoanions with high affinity in a 1 : 1 stoichiometry by virtue of forming H-bonds with ten inward-pointing H-atoms. And they not only bind but also efficiently transport them across lipid bilayers. Among macrocycles studied, **8** exhibits high selectivity in transporting chloride ions with a selectivity ratio of $Cl^-:Br^-:I^-$ = 17.8 : 1.6 : 1, a sequence inversely proportional to its binding affinity. Such high transport selectivity surpasses those of synthetic Cl^- carriers[83] and even native channels such as the ClC-1 Cl^- channel[84] (with a transport selectivity of $Cl^-:Br^-:I^-$ = 5 : 2 : 1), which is quite remarkable. The compound **8** is able to transport anions across lipid bilayers with a high chloride

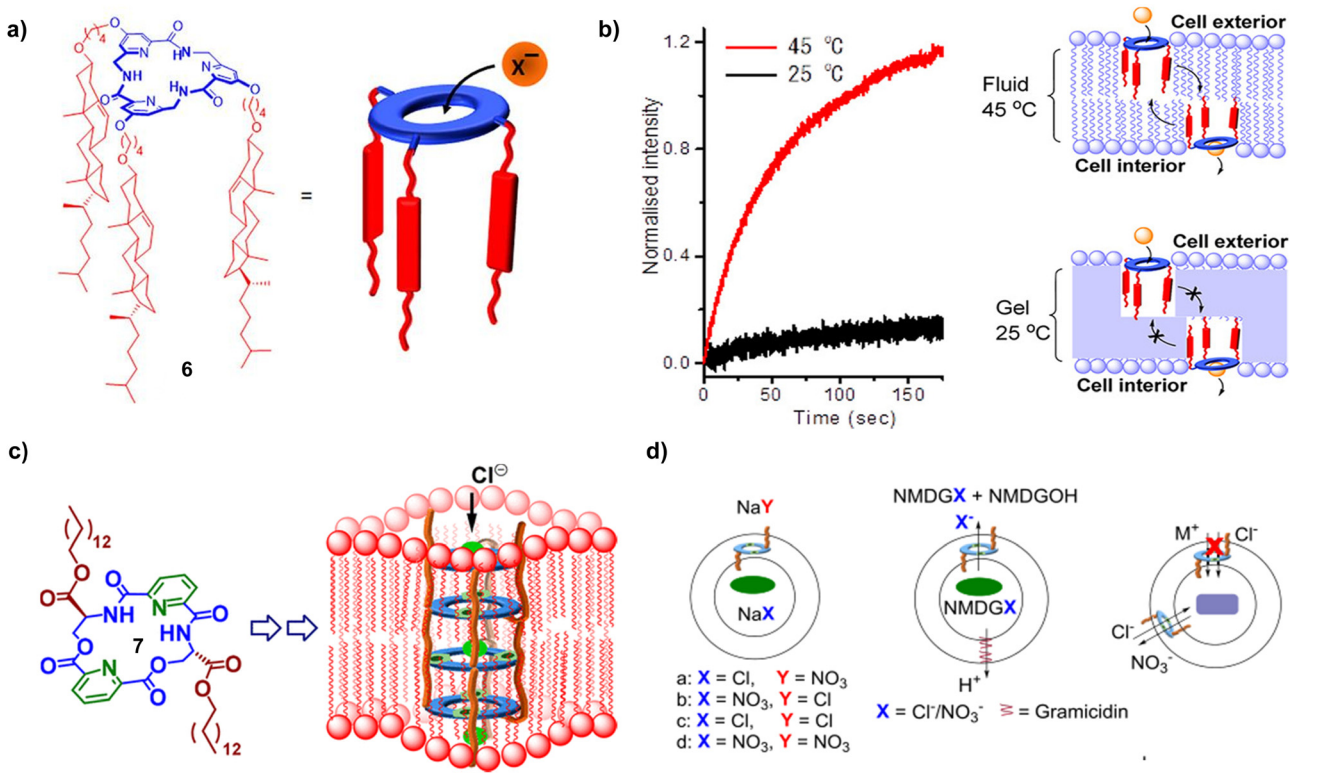

Fig. 9 (a) Schematic representation of the cholesterol appended macrocycle **6**, the best transporter. (b) Variable temperature HPTS assay with macrocycle **6** (23.1 μM) to illustrate carrier mechanism. (d) Chemical structure of compound **7**. (d) Assays to determine the mechanism of chloride transport (symport/antiport). Reproduced with permission from ref. 79 (Copyright 2017 The American Chemical Society) and ref. 81 (Copyright 2020 The American Chemical Society).

selectivity and restore the depleted airway surface liquid of cystic fibrosis airway cell cultures.

As early as 2012, Gong and his co-workers has shown that the amide installed around the macrocyclic exterior can work with aromatic π–π stacking interactions guide the macrocycles to generate self-assembled channels having sub-nanometer pores with unique transport properties (Fig. 10(b)).[85] These nanotubes possess modifiable surfaces and internal pores of a uniform diameter defined by the constituent macrocycles, enabling not only highly selective transmembrane ion transport where the H^+/Cl^- selectivity ratio exceeds 3000, far surpassing natural proton channels such as the influenza virus M2 protein (P_{H^+}/P_{Cl^-} = 19.7).[87] Additionally, channel **9** also demonstrates significant selectivity for potassium ions, with an H^+/K^+ selectivity ratio of about 2000. Furthermore, **9** displays highly efficient transmembrane water permeability, with the estimated single channel water permeability of 2.6 (± 0.4) × 10^{-14} cm^3 s^{-1} that is about 22% of that of AQP1/CHIP-28 (11.7 × 10^{-14} cm^3 s^{-1}).[88] This work confirms that hydrophobic nanopore of suitable sizes can exhibit high water transport efficiency.

In 2023, Lu's group reported an innovative strategy for constructing molecular nanotubes **10** by covalently linking multiple hexakis (*m*-phenylene ethynylene)-based macrocycles *via* a amide-containing flexible linker (Fig. 10(c) and (d)). This linker provides H-bonds that results in constrained face-to-face stacking stacking among the macrocycles, leading to molecular nanotubes with specific length and structure.[88] Having a non-deformable internal pore, these molecular nanotubes exhibit excellent ion transport capabilities. The ion transport properties of **10a** and **10b** show a trend directly related to the number of macrocycle units in the molecule, with **10b** that has four macrocycle units exhibiting higher thermodynamic stability and better transport ability than **10a**. Notably, **10b** efficiently transports both K^+ and H^+, displaying a channel opening time of greater than 60s, far surpassing *m*-PE macrocycle **9** that forms channels *via* non-covalent H-bonds. This high channel opening time is likely due to covalent actions that anchor multiple stacked macrocycle units, lowering the entropic barrier to forming transmembrane channels and thereby enhancing the channel's thermodynamic stability. This work may aid in future design and construction of molecular nanotubes with specific length and higher stability.

3. H-bond-rigidified helical foldamers as ion transporters

Zeng *et al.* conducted an in-depth study of the design and characteristics of helically folded pyridine-derived aromatic oligoamides of 2.8 Å in diameter. Utilizing the directionality and stability of H-bonds, they successfully designed and

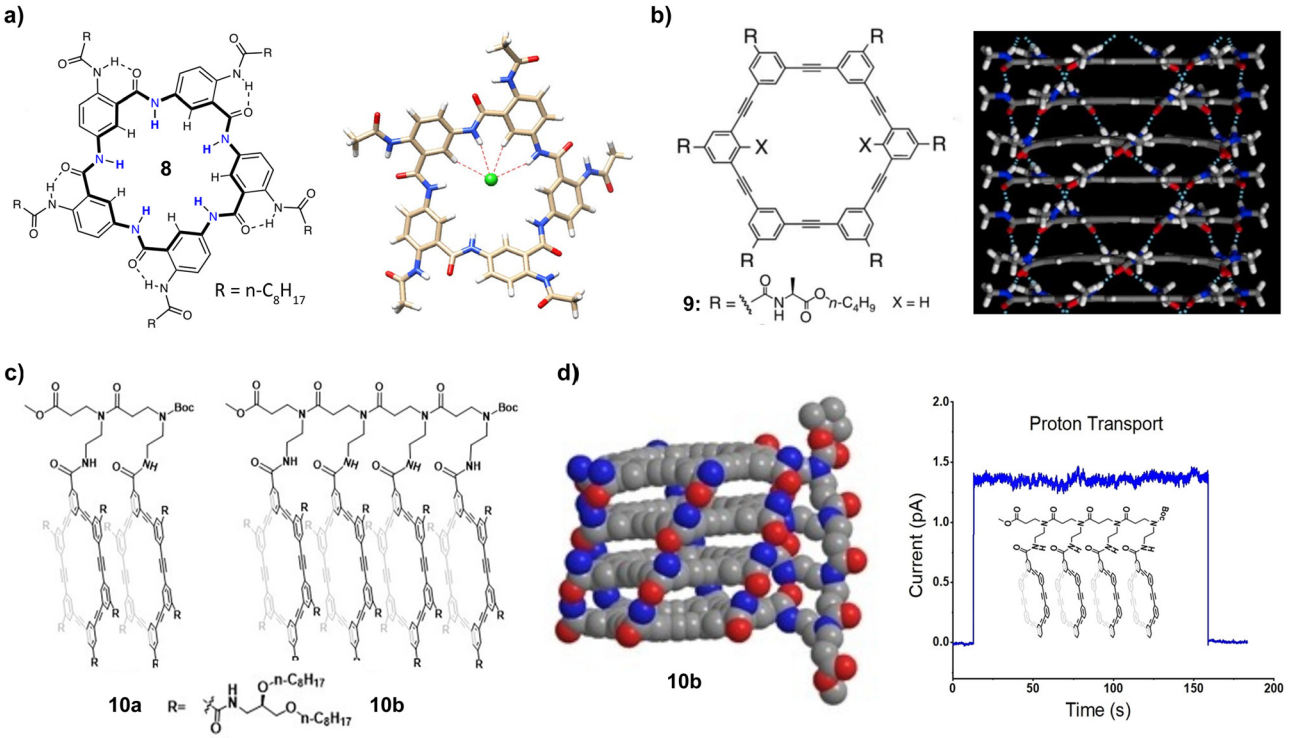

Fig. 10 (a) Chemical structure of pentameric macrocycle **8** and its complex with Cl^- anion. (b) Structure of macrocycle **9** and the corresponding self-assembled nanochannel *via* H-bonds formed around the exterior. (c) Structures of **10a** and **10b**. (d) The computationally optimized structure of **10b** and its single channel current traces of proton transport at 200 mV in HCl (2.0 mM at 20 °C). Reproduced with permission from ref. 82 (Copyright 2023 Springer Nature), ref. 85 (Copyright 2012 Springer Nature) and ref. 86 (Copyright 2023 Wiley).

synthesized a series of oligoamides, with specific conformations and functionalities (Fig. 11). Using computational molecular modeling, they design and validate a new type of pyridine-based folding oligoamides, characterized by having about four repeating units per helical turn (Fig. 11(b)–(d)).[89] Intended for recognition of water molecules in their helical cavity, corresponding crystal structure of **12** indeed reveals encapsulation of both conventional and unconventional water dimers within its cavity of 2.8 Å in radius (Fig. 11(c)).[90] Within the unconventional water dimer, two water molecules interact through an unusual H–H interaction (2.25 Å) instead of a typical H-bond. This crystal structure further shows how the molecule forms a specific folded structure through an internal H-bond network to accommodate water molecules (Fig. 11(c)).

Although **12** can bind water molecules with good affinities, the packing of these water complexes is not favorable for creating 1D hollow tubular cavities to encapsulate 1D water chains. Zeng *et al.* recently hypothesized that incorporating two electrostatically complementary functional groups at the ends of the helices may efficiently align short helices to form one-dimensionally aligned helical chiral stacks. If the helical molecules have a cavity, this 1D packing should create a hollow tubular cavity for guest molecule inclusion. To Test this hypothesis, pentamer 13 with complementary ''sticky'' groups at the two helical ends was designed and made (Fig. 11(d)). Computational and experimental results confirm that these folding oligoamides spontaneously undergo chiral crystallization, forming homochiral helical structures *via* complete overlap of the aromatic frameworks and weak H-bonding between terminal groups (Fig. 11(e)). Such seamless integration of short helices into long nanotubes allows for enclosing chains of MeOH or CH_2Cl_2 molecules in the hollow cavity (Fig. 11(e)).[91] This interesting piece of work not only opens new avenues for designing new types of chiral materials for chiral recognition, but also forms the basis for the design of powerful artificial water channels.

Interestingly, soaking the MeOH-containing crystals of **13** in water-containing solvents reveals that only 24–40% of the MeOH molecules inside were replaced by water. This is in stark contrast to other analogous oligomers like **12**, which can accommodate two water molecules in their cavity. This suggests that the hollow cavity in **13** is functionally selective and has a higher binding affinity for methanol or dichloromethane than for water molecules. This further indicates that water binding by these pyridine oligomers may strongly depend on the end groups, oligomeric length, and even exterior side chains. Therefore, Zeng and his co-workers carried out systematic structural modifications in oligomeric length, repeating units, or end groups. These efforts firstly led to identification of **14** (Fig. 12(a)–(c)).[92] Similar to **13**, the H-bonding of the ''sticky'' end groups mediates the formation of a one-dimensional helical structure, resulting in a hollow, tubular water channel (Fig. 12(a) and (b)).

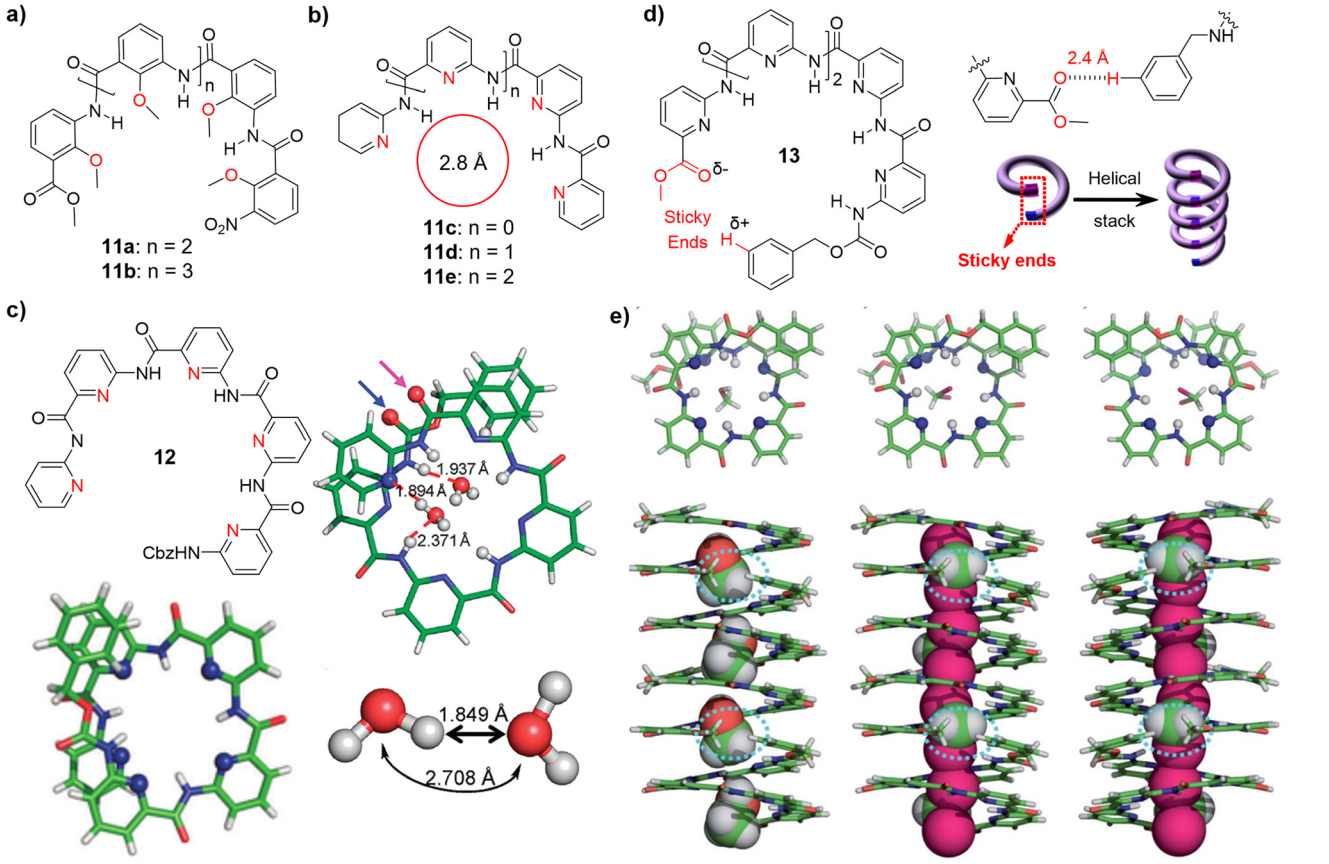

Fig. 11 (a) Methoxybenzene-based pentamer **11a** and hexamer **11b**. (b) Pyridine-based oligomers **11**, having an interior water-binding cavity of 2.8 Å in diameter. (c) Structure of **12** and crystal structure having a a water dimer in its cavity. (d) The structure of elical foldamer **13**, illustrating a "sticky end" approach for building helical channels from short helices. (e) Crystal structures and 1D columnar packing by helically folded **13** containing either MeOH or CH_2Cl_2 in their helical interiors. Reproduced with permission from ref. 89 (Copyright 2011 The Royal Society of Chemistry), ref. 90 (Copyright 2011 The American Chemical Society) and ref. 91 (Copyright 2012 The Royal Society of Chemistry).

An unusual observation emerged when the particle sizes of **13**-containing large unilamellar vesicles (LUVs) were examined using dynamic light scattering analysis (Fig. 12(c)). The obtained results suggest that the water-transporting ability of **13** likely lead to initial swelling of the LUVs, increasing the internal pressure and subsequently causing rapid vesicle fusions to produce larger LUVs of 350 nm or more. These data highlight the crucial roles played by both the well-aligned 1D water chains and the proton gradient, working together to create "osmotic pressure" that facilitates the transport of water molecules across the membranes. The idea of "proton gradient-induced water transport" is particularly intriguing, as no other synthetic systems for proton or water transport have demonstrated this unusual behavior thus far.[92]

A very surprising discovery was made in 2020 when Zeng and his co-workers test another structurally similar pentamer **15** (Fig. 12(d)).[93] With its internal hollow cavity of approximately 2.8 Å that matches the size of AqpZ's central pore, stacked **15** demonstrates high water transport (around 3×10^9 H_2O s^{-1} $channel^{-1}$) and effective rejection of salts like NaCl and KCl. This high selectivity is attributed to the narrow dimensions within the channel and the lack of binding elements that release the ionic hydration shell, collectively ensuring that only water molecules can pass through while salt ions are effectively blocked. And the exhibited high water permeability is more than 70 times higher than all previously reported artificial water channels with high salt rejection. This makes channel **15** the first artificial water channel with aquaporin-like features in water transport, demonstrating the significant utility of a "sticky end"-mediated molecular strategy. Interestingly, having a slightly reduced internal pore volume (by about 20% relative to **15**, Fig. 12(e)) and similar interior surface functionality, **14** shows a 15-fold decrease in the water transport rate compared to **15**. This contrast in performance between the two channels highlights (1) an increased degree of freedom for water molecules and a reduced deviation from the optimal H-bonded structure as the two influential factors for designing artificial synthetic water channels to enhance water permeability, and (2) the anomalous water transport behaviors in angstrom-scale hollow pores, making them an ideal pair for testing existing and emerging computational algorithms to predict water transport properties of narrow pores at or below the nanometer scale.

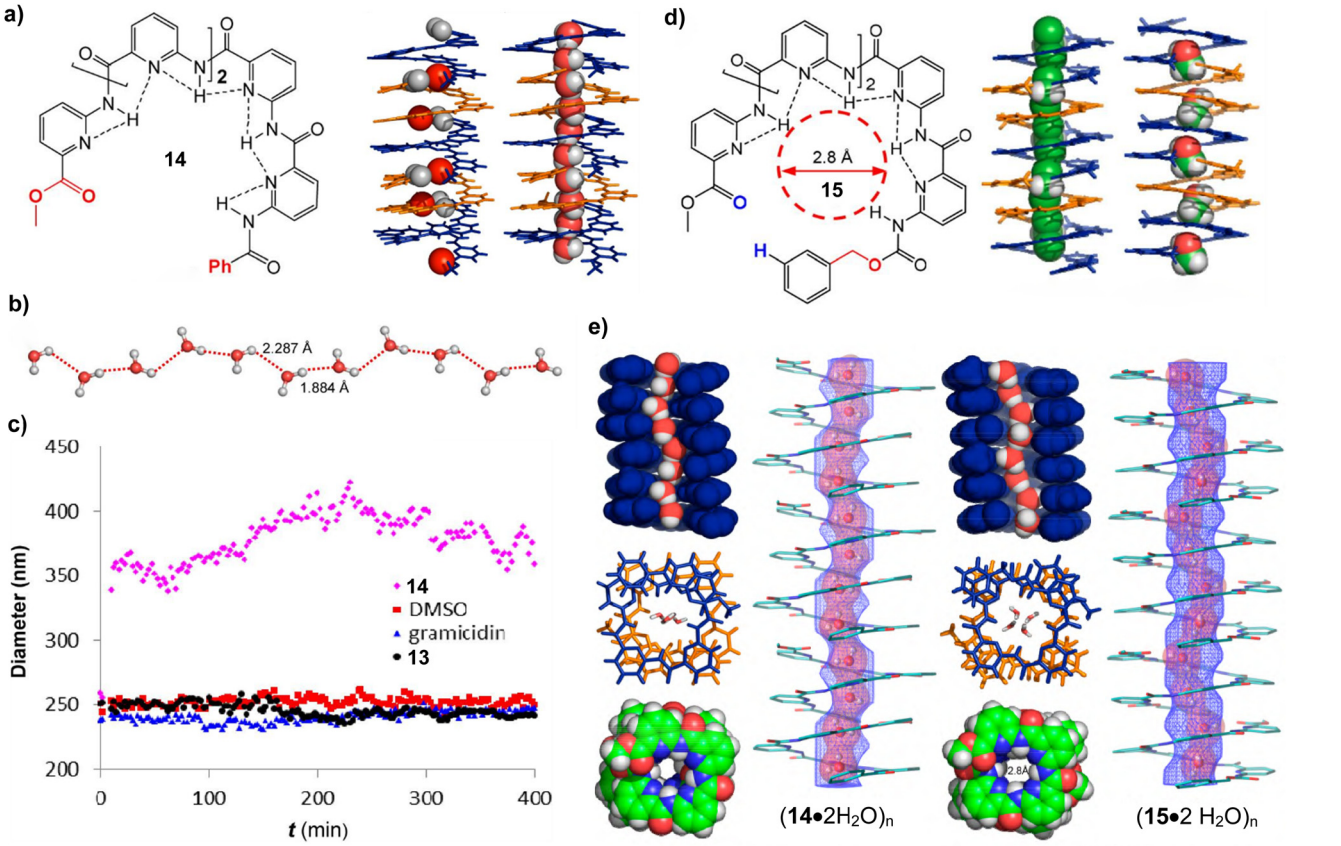

Fig. 12 (a) Chemical and water chain-containing crystal structures of **14**. (b) H-bonded 1D water chain in **14**. (c) Dynamic light scattering experiments, revealing Proton gradient-induced enlargement in diameter of LUVs containing channel **14** that is indicative of water transport by **14**. (d) Chiral aquapores of ~2.8 Å across for accommodating CH_2Cl_2 and MeOH molecules by **15**. (e) Water chain-containing crystal structures of **14** and **15**, suggesting the internal volume of **14** is about 20% smaller than that of **15**. Reproduced with permission from ref. 92 (Copyright 2014 The American Chemical Society) and ref. 93 (Copyright 2020 The American Chemical Society).

To reduce synthetic complexity of pyridine oligoamides such as **15** that ends up with <1% in overall yield, in another study, Zeng *et al.* reported $POCl_3$-mediated one-pot polymerization protocol for efficiently generating polypyridine amide foldamer channels **16** of 2.8 nm in helical height at yield of up to 50% (Fig. 13(a)).[94] This is the first example of fully H-bonded aromatic amide foldamer-based long organic nanotubes greater than 1 nm, which are rapidly synthesized from their constituent folding codons *via* one-pot polymerization.

Synthetically, this method is simple and efficient, but its identification took years in that only when the amount of $POCl_3$ increases to fifty equivalents at high temperature of 85 °C, sufficiently long $\mathbf{P_{31}}$ that has a molecular weight 7.7 kDa and contains 31 repeating units can then be produced. MD simulations suggest the formation of a single-file water chain inside channel $\mathbf{P_{31}}$, providing a chemical environment for the rapid transport of water molecules and protons. Experimental results show that the polymeric channels $\mathbf{P_{31}}$ promote rapid and highly selective transport of 1.6×10^9 H_2O s^{-1} $channel^{-1}$ while transporting protons as fast as gA, with extremely high rejection of ions (Na^+, K^+ and Cl^-) during water and proton transport.

In 2014, Li *et al.* introduced a series of H-bonded hydrazide-linker helical aromatic oligomers and polymers containing phenylalanine tripeptide chains capable of efficiently inserting into lipid bilayers to aid in the formation of single-molecule channels. (Fig. 14(a)).[95] These artificial transporters mimic and even surpass the ion transport properties of gA in some aspects, demonstrating the potential of artificial ion channels. Oligomers **17b–17e** display high NH_4^+/K^+ selectivity as NH_4^+ readily forms intermolecular H-bonds with carbonyl O-atoms within the helical cavity in addition to electrostatic interactions. As the helical backbone is extended further, the selectivity for NH_4^+/K^+ significantly improves, supporting the important role of intermolecular H-bonds in enhancing NH_4^+ transport. Aside from high selectivity for NH_4^+/K^+, longer oligomer **17d** and polymer **17e** even surpasses gA in terms of NH_4^+ transport speed. Notably, **17b** demonstrates high efficiency in transporting Tl^+ ions at a rate comparable to gA. As the helical backbone length increases, the rate of Tl^+ transport decreases, likely as a result of electrostatic "drag" by the channel wall. The study further reveales determinants of channel selectivity, including the dehydration energy of ions and the length of the helical backbone. The selectivity order for alkaline cations matches the

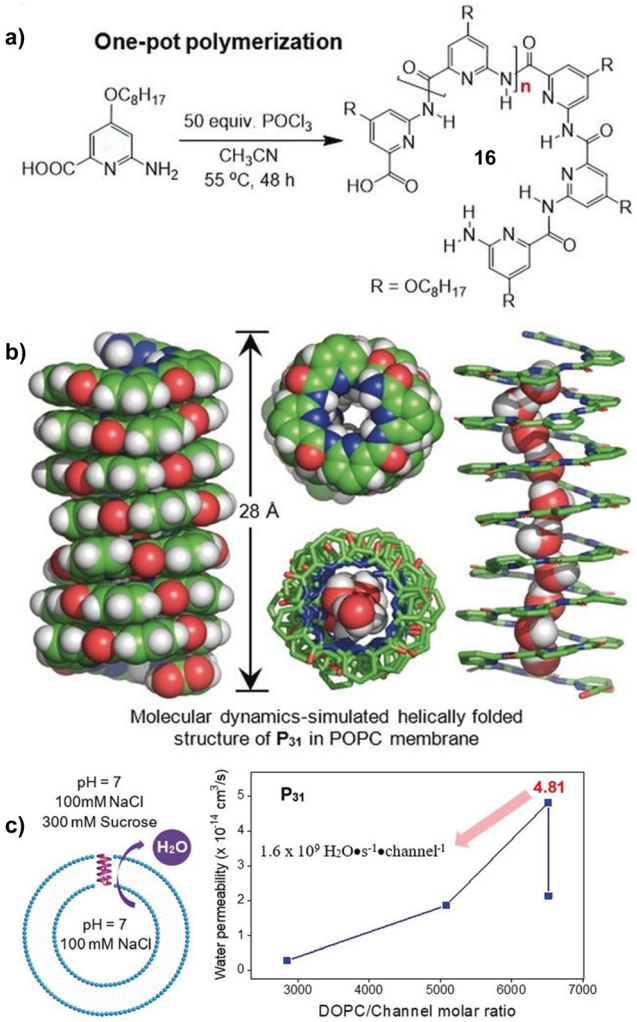

Fig. 13 (a) One-pot synthesis of H-bonded amide-linked polypyridine channels **16**. (b) Molecular dynamics-simulated structure of **16** (n = 31, $\mathbf{P_{31}}$) made up of 31 repeating units in POPC membrane, revealing the ability of polypyridine channel to host 1D water chains for mediating possible transport of protons and water molecules. (c) DOPC-based LUVs under hypertonic conditions (300 mM sucrose) for quantifying water permeability of $\mathbf{P_{31}}$ at different lipid/channel molar ratios. Reproduced with permission from ref. 94 (Copyright 2020 Wiley).

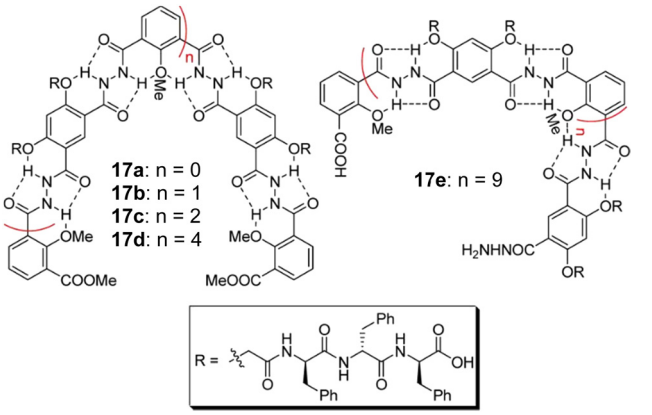

Fig. 14 Structures of oligomers **17a–17d** and polymer **17e**. Reproduced with permission from ref. 95 (Copyright 2014 The American Chemical Society).

Eisenman sequence, which reflects the energy changes during the ion dehydration process.

However, the large dimensions of the triphenylalanine side chains (9 × 11 Å) seen in **17** are incompatible with the typical aromatic π–π stacking distance of 3.4 Å, potentially distorting the central helical backbone and affecting its intrinsic ion transport properties. This consideration led Zeng to synthesize longer polymers with only straight alkyl chains on the exterior to better assess the true ion-transporting properties of these channels. In this regard, by polymerizing two easily accessible repeating units using HATU, A and B, they successfully produced longer polymeric foldamers **18**, with helical heights ranging from 2.1 to 14 nm and a cavity diameter of about 6.5 Å (Fig. 15(a)).[96] This is the first time that fully H-bonded aromatic foldamers can be made to exceed 2 nm in height. Expectedly, the alkyl-chain-appended polymers **18** selectively transport anions across lipid membranes, which is contrary to Li's earlier report of preferred cation transport over anions. Particularly, polymer channels having octyl side chains and a helical height of 3.6 nm transport iodide ion ten times faster than that of chloride ions.

It is somewhat puzzling to note that the internal surfaces of **18** are covered with electron-rich O-atoms, yet they exhibit high selectivity for anions over cations. The analysis of equilibrium MD trajectories reveals the average electrostatic potential inside the channel's central lumen to be positive, originating from the numerous methyl groups lining the lumen. This explains the channel's selectivity for anion transport. Further, even in cholesterol-rich environments, these channels still maintain high iodide ion transport activity, demonstrating an EC_{50} value of 0.37 mM. This is particularly important for medical applications, as cholesterol-rich environments can affect the efficacy of drugs.

Very recently, Zeng *et al.* found that lipid anchors (**LA**) introduced at the helical ends convert anion channels **18** into powerful artificial water channels **19-LA** (Fig. 15(b)),[40] replicating water transport function of AQPs by utilizing a set of selectivity principles and structural motifs distinct from those in AQPs. Specifically, they found that (1) a large, hollow tubular cavity with a pore diameter significantly larger than that of a water molecule (2.5 Å) but still smaller than a Na^+ ion with its first hydration shell (~9 Å) can compete well with AQPs, (2) high water transport does not necessarily use the single-file arrangement as seen in AQP1 and other channels, and (3) high salt rejection with these large pores can be achieved by lining the interior pore surface with hydrophobic functional groups such as alkyl groups that are ineffective at replacing ion-coordinated water molecules. As such, having its interior surface decorated by many ethyl groups, **19b-LA** transports water at an extremely high rate of 2.7×10^{10} H_2O s^{-1} $channel^{-1}$—2.5 times that of the aquaporin AQP1—while rejecting salts (NaCl and KCl) and even protons. Exploring the mechanisms of proton rejection using MD simulations, they found that

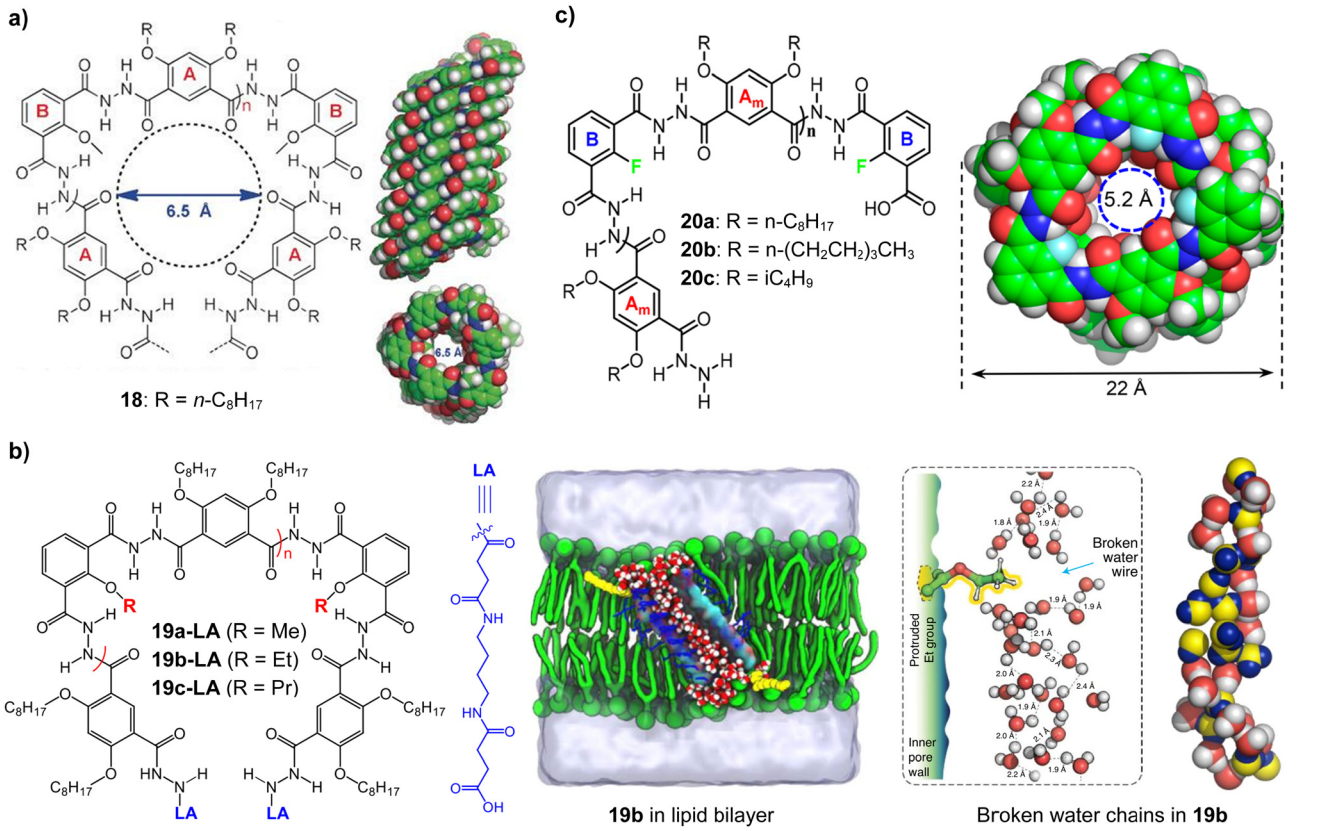

Fig. 15 (a) Foldamer-based approach for constructing H-bonded pore-forming polymeric anion channels **18**, having a hollow cavity of 6.5 Å in diameter after excluding van der Waals volume of atoms decorating the channel's interior. (b) Chemical structures of ultrafast artificial water channels **19-LA**; broken water chains computationally observed in **19b** accounts for why **19-LA** rejects protons. (c) Superfast fluorine-decorated artificial water channels **20** and its quantum mechanics-computed helically folded tubular structure at the HF/6-31G(d) level. Reproduced with permission from ref. 40 (Copyright 2021 Springer Nature), ref. 96 (Copyright 2020 Wiley) and ref. 97 (Copyright 2022 The American Chemical Society).

fluctuation of the internal hydrophobic alkyl groups blocks the formation of channel-spanning water chain, thus preventing proton transport. This mechanism of proton blocking is unprecedented in nature and offers a new perspective on the design of artificial water channels.

It is worth pointing out that **19b-LA** needs lipid anchors to properly align and achieve ultrafast water conduction. Otherwise, its water transport rate plummets by 75% to around 0.6×10^{10} H_2O s^{-1} $channel^{-1}$. To overcome this limitation, Zeng *et al.* explored the possibility of using electron-withdrawing fluorine atoms to influence channel structure and guest binding behaviors (such as water and ions) by reducing the interior pore size from 6.5 to 5.2 Å and increasing channel wall smoothness due to fluorine's low lone pair donation tendency (Fig. 15(c)).[97] Electronic property of the latter leads to minimized intermolecular host–guest H-bond interactions with water molecules and coordination bonds with cations. With an average channel length of 2.8 nm and a pore size of 5.2 Å, **20a** is the top performer among the studied flurofoldamers, achieving an impressive water conduction rate of 1.4×10^{10} H_2O s^{-1} $channel^{-1}$ while nearly completely rejecting salt ions (Na^+, K^+ and Cl^-) and protons. These findings highlight the beneficial impact of incorporating $C(sp^2)$–F moieties on the inner surfaces of foldamer-based water channel pores, introducing new principles for channel design that may inspire further advancements in membrane technologies for water desalination, nanofiltration, and medical dialysis.

In the same year, they also investigated the membrane-related function of pyridine–pyridone foldamer channels **21** (Fig. 16(a)).[98] Among the six amide coupling agents tested, only PyBOP gives rise to sufficiently long polymer channel **21d**, reaching a length of 3.4 nm. A key feature of these artificial channels is their nanoscale carbonyl-decorated tubular pore of only 3 Å wide, which allows for highly selective and rapid proton transport. Compared to known channels like gA and the M2 protein channel, **21d** demonstrates a proton conduction rate of 253 pS that was 0.22 and 10 times faster, respectively. Remarkably, **21d** also exhibits extremely high selectivity in repelling water molecules and ions including Cl^-, Na^+, and K^+, with selectivity factors of 167.6, 122.7, and 81.5, respectively. To account for proton rejection, the researchers proposed a novel proton transport mechanism where protons may facilitate the formation of channel-spanning water chain from two or more short ones, creating the pathway for their subsequent transmembrane transport (Fig. 16(b)). This mechanism still follows the Grotthuss mechanism,[99] which involves the rapid

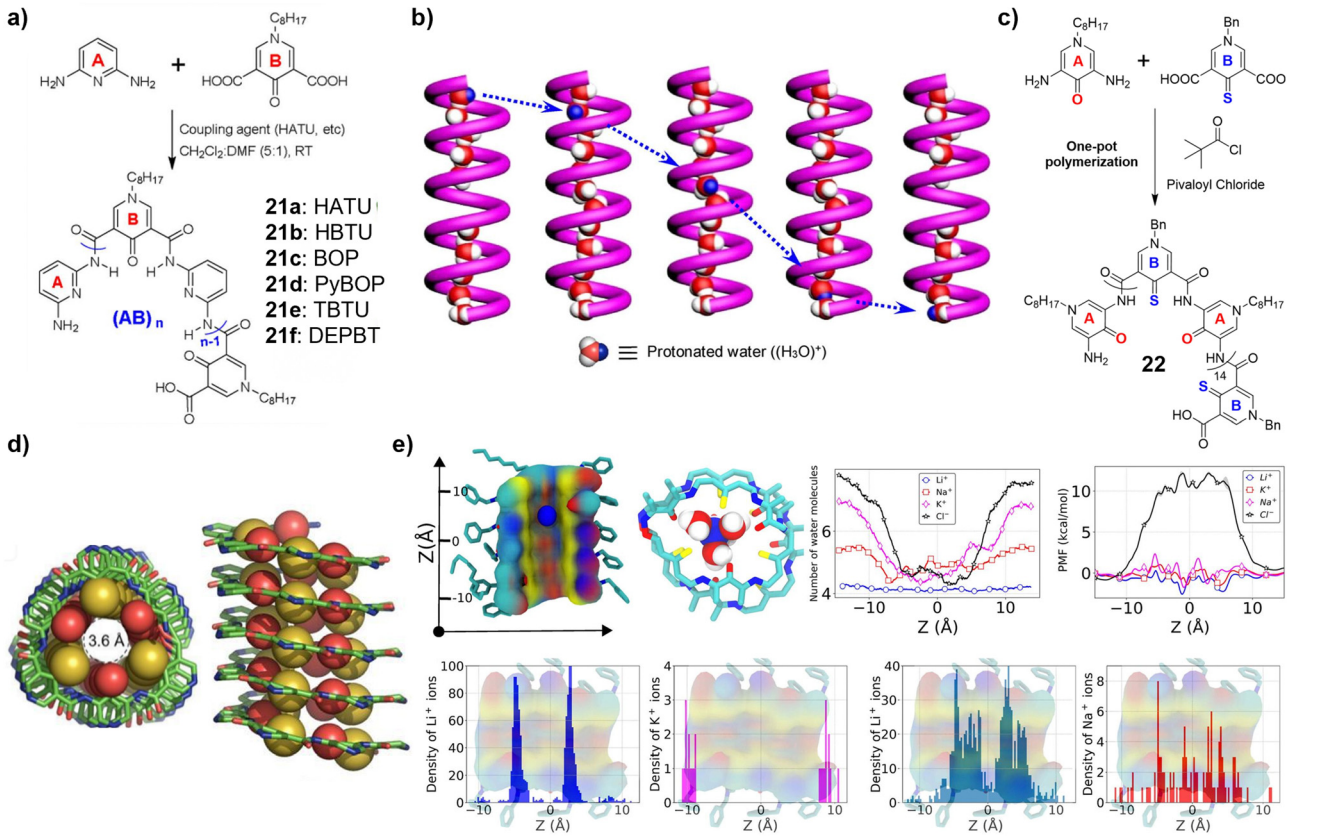

Fig. 16 (a) Structures of AB type polymeric channels **21**. (b) A mechanism for proton transport mediated by a proton wire created by the proton itself. (c) Molecular design and structure of foldamer-derived lithium channels **22**. (d) MD-optimized backbone scaffold of **22**. (e) MD simulations of selective ion permeation through channel **22**. Reproduced with permission from ref. 98 (Copyright 2022 Wiley) and ref. 100 (Copyright 2023 Wiley).

diffusion of protons along a chain of water molecules connected by H-bonds, but it entails proton-induced formation and breaking of water chains, rather than relying on a pre-existing continuous water chain.

Utilizing pivaloyl chloride as a mild one-pot polymerization agent, Zeng *et al.* invented another class of sulfur-containing foldamer-based artificial lithium channels **22**,[100] a nanoscale channel with a unique structure and functionality that efficiently and selectively transports Li^+ ions (Fig. 16(c)). The core feature of **22** is its unique structural design, consisting of internally H-bonded sulfur-containing aromatic foldamers that form a hollow cavity with a diameter of 3.6 Å (Fig. 16(d)). This design provides an ideal channel size and right chemical environment for Li^+ transport. When embedded in lipid bilayers, **22** transport Li^+ highly efficiently, with lithium conduction rate of 18.4 pS. This high rate is comparable to that of gA in transporting K^+ ions. It also transports Li^+ extremely selectively, with selectivity factors of 15.3 and 19.9 for Na^+ and K^+ respectively. Computational simulations reveal the molecular-level structure of **22** and its selective permeation mechanism of Li^+. The simulations show that water molecules and sulfur atoms within **22** synergistically work together to facilitate the transport of Li^+, while the channel size effectively excludes Cl^- ions and other larger alkali metal ions (Fig. 16(e)).

Liu's group studied transport function of quinoline-derived transmembrane nanochannel **23** (Fig. 17(a)),[101] featuring an extremely small cavity of only 1 Å in diameter as reported by Huc in 2003.[102]

This small cavity size coupled with high ionic desolvation energies enables the channel to effectively block the permeation of cations, anions and water molecules, while allowing only protons to pass through. Its ultra-fast proton transport capability is clearly evidenced from its high proton flow rate, reaching 10^7 H^+ s^{-1} channel^{-1} that is comparable to that of gA. Research into the proton transport mechanism uncovers that the directionally and sequentially aligned NH-chain is crucial for proton flux, providing a highly efficient pathway for proton transfer without a need for 1D water chain. This discovery offers new perspective and strategy for the design of artificial proton channels.

Wu's group designed a new class of anion channels built from *m*-pyridine-urea groups as represented by **24** (Fig. 17(b)).[103] These oligomers fold through intramolecular H-bonding between the pyridine N-atoms and urea NH group. The uniqueness of this folding system is that not all urea H-atoms participate in forming intramolecular H-bond as verified by the crystal structure of a short trimer. In **24**, multiple strong intramolecular H-bonds formed twist the otherwise linear

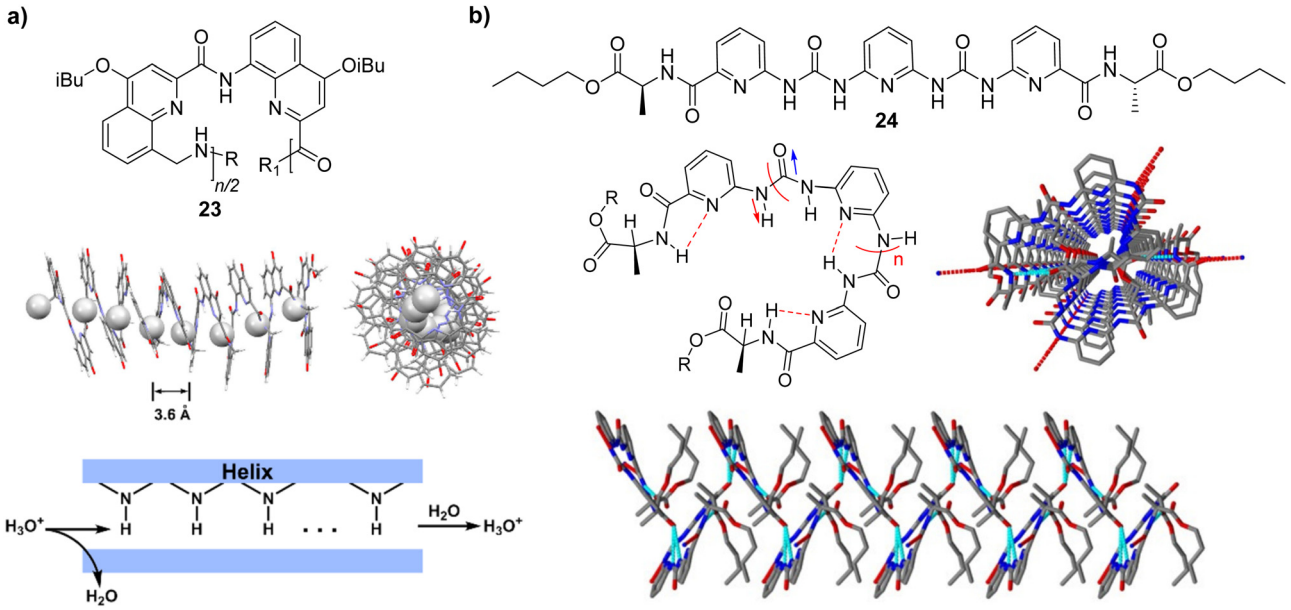

Fig. 17 (a) Structure of foldamer-derived proton channel **23** (n = 16, R = Boc, R_1 = Me) and the corresponding proton transport mechanism *via* the single-file NH-chain inside the luminal cavity. (b) Structure of aromatic oligoureas as represented by **24** rigidified by intramolecular H-bonds and its crystal structure that illustrates a 1D channel for anion transport. Reproduced with permission from ref. 101 (Copyright 2021 The American Chemical Society) and ref. 103 (Copyright 2021 Wiley).

backbone into a twisted planar structure, forming a pseudo-macrocyclic ring; 2D NMR experiments have confirmed the presence of such a pseudo-macrocyclic ring in solution, with the orientation of the carbonyl and NH groups being consistent in both solid and solution state. Having a twisted planar structure, **24** readily self-assembles to create nanochannels where the urea carbonyl groups are oriented outward and the NH groups inward. This leads to optimized pathway for electron-rich small-sized anionic species and thereby efficiently transport chloride ions while repelling other anions such as bromide and nitrate ions. This work provides an interesting supramolecular system for designing new, efficient and highly selective biomimetic anion channels.

In 2021, Dong *et al.* introduced a novel type of anionic transmembrane nanochannel, constructed through dynamic covalent reactions involving hydrazine and dialdehyde units to create dynamic covalent helix **25** of 1 nm in cavity diameter (Fig. 18(a)).[104] **25** was synthesized using a one-pot dynamic covalent chemistry strategy and was found to self-assemble into helical nanotubes through intramolecular H-bonding and aromatic π–π interactions. These nanotubes feature nanoscale hollow cavities, providing stable and sizable channels for ion transport. **25** significantly accelerates the transmembrane transport of anions, with a selectivity order of $I^- > Br^- > Cl^- > SO_4^{2-}$ (Fig. 18(b)). Its high transport activity can be manifested by its low half-maximal effective concentration (EC_{50}) value of only 0.08 mol%.

As early as 2012, Jeong's group designed and synthesized a series of folding molecules **26** that mimic the key H-bonding pattern of the ClC chloride ion channel (Fig. 18(c)).[105] These H-bond-rigidified molecules are characterized by their ability to bind Cl^- ions precisely through four H-bonds (two formed with urea NHs and two with terminal OHs), a unique binding mode achieved by incorporating specific urea and hydroxyl groups into the molecular backbone. These four H-bonds collectively create a cavity capable of stabilizing Cl^- ion. The crystal structure analysis of the complex formed with tetrabutylammonium chloride confirmed that the binding site of the synthetic molecule is similar to that found in the ClC chloride ion channel (Fig. 18(d)). Notably, **26a** demonstrates superior Cl^- transport efficiency among all the tested molecules. This enhancement in efficiency is attributed to the side chains of **26a**, enhancing its lipophilicity to achieve a possibly better balance between lipophilicity and hydrophilicity, thereby improving its mobility in the lipid bilayer. Additionally, the chloro group in **26a** may enhance the H-bonding capability of the urea NHs through an electron-drawing effect, increasing the binding affinity for Cl^- ion. Furthermore, the transport mechanism of **26a** was confirmed to be through Cl^-/NO_3^- exchange, a counter-transport mechanism.

Two years later in 2014, Jeong's group reported MCl-selective symporters **27** that can selectively transport NaCl or KCl across phospholipid membranes.[106] Symporters **27** consist of two heterogeneous binding sites: one for binding chloride ions and another for binding alkali metal cations (Fig. 18(e)). Through cooperative actions, this molecular design significantly enhances the binding capacity for chloride ions in the presence of Na^+ or K^+ ions (Fig. 18(f)). The uniqueness of these symporters lies in their high structural modulability and selectivity achieved by adjusting the size of the azacrown ethers in the symporters to fit different sizes of cations. Specifically, **27a** incorporates 15-azacrown-5 as its cation binding site and

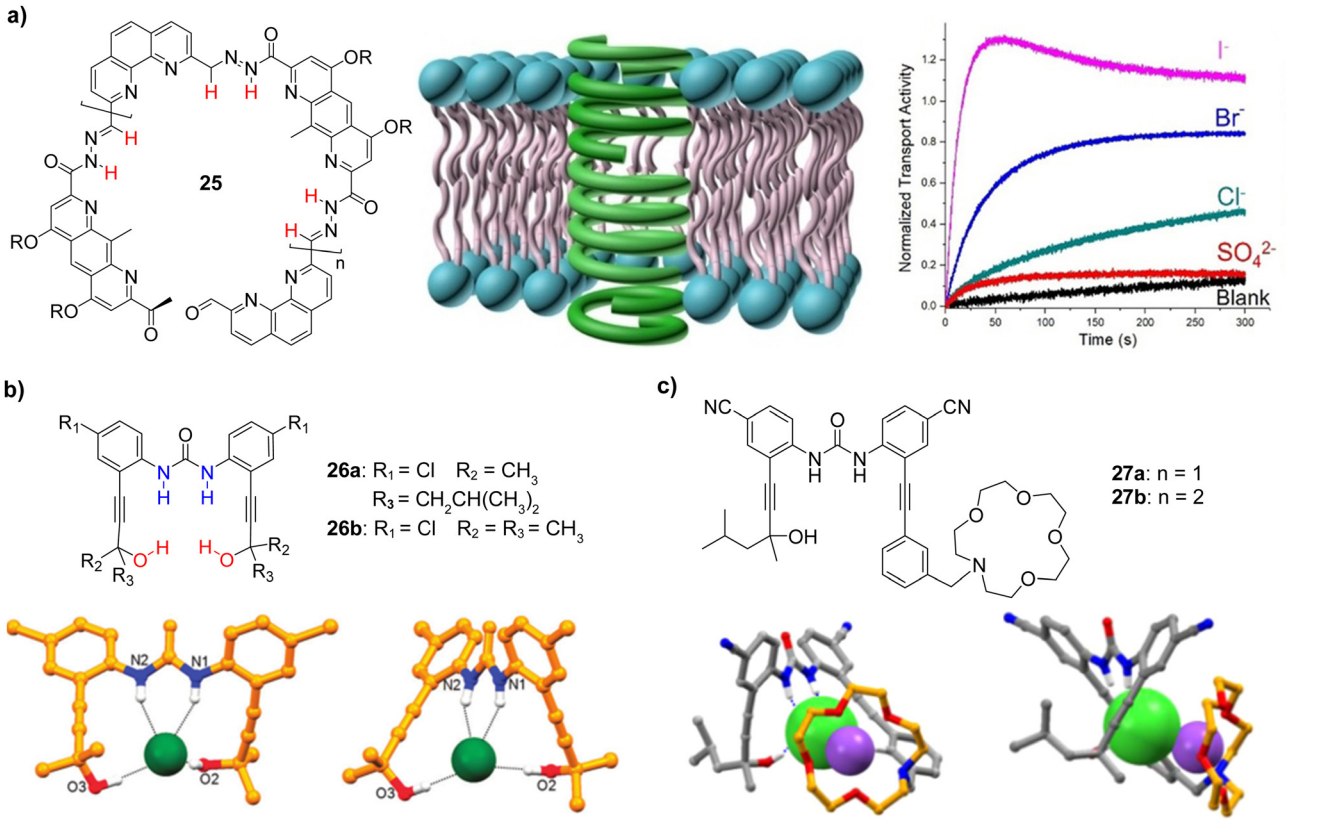

Fig. 18 (a) Transmembrane channels formed by dynamic covalent helixs **25** in the lipid bilayer and its anion transport selectivity. (b) Chemical structures of **26** and the two views of the crystal structure of **26b** with tetrabutylammonium chloride. (c) Chemical structures of symporters **27** and the two views of the crystal structure of a complex formed between **27a** and sodium chloride. Reproduced with permission from ref. 104 (Copyright 2021 Wiley), ref. 105 (Copyright 2012 The Royal Society of Chemistry) and ref. 106 (Copyright 2014 The American Chemical Society).

exhibits moderate selectivity for NaCl, promoting transport of NaCl across phospholipid membranes by forming contact ion pairs. On the other hand, 18-azacrown-6 as its cation binding site endows **27b** with strong selectivity for KCl, facilitating transport of KCl. This design strategy enables the symporters to somewhat mimic the function of natural symport proteins, specifically those that simultaneously transports cations and anions through an M^+/Cl^- cotransport mechanism (Fig. 18(g)).

In 2014, Jiang *et al.* described a new class of aromatic triazole foldamers **28** (Fig. 19(a)).[107] The core feature of **28** is its fully pre-organized conformation maintained by two peripheral intramolecular H-bonds between the amide NH and the N^2/N^3 atoms of each triazole. These H-bonds allow **28** to form a crescent-shaped cavity even in the absence of guest molecules, with a shape and weak H-bond donor arrangement pre-adapted for chloride ion binding. This fully pre-organized conformation is key to the high-efficiency transport of chloride ions by **28a.** In contrast, **28b** is designed to have a group occupying the internal cavity and additionally forcing the molecule to take a more loosely coiled conformation. NMR titration experiments show that the binding constant of **28a** for chloride ions is much higher than that of **28b** (Fig. 19(b)).

Very recently, Talukdar *et al.* reported a series of novel triazole-cyanostilbene receptors as represented by **29** (Fig. 20(a)), which

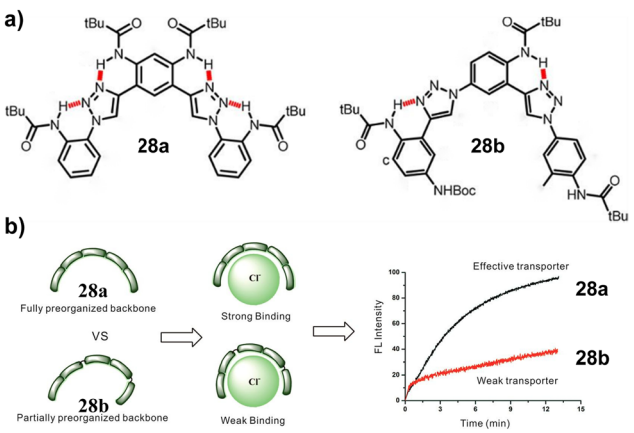

Fig. 19 Molecular design of triazole foldamers **28**. (b) Cartoon illustration of **28** binding with chloride ions and a schematic diagram of their ion transport activity. Reproduced with permission from ref. 107 (Copyright 2014 The American Chemical Society).

significantly enhance the recognition and the efficiency of transmembrane transport of anions through their unique multivalent C–H···anion H-bonding interactions.[108] These receptors are designed to combine 1,2,3-triazole, cyanostilbene, and electron-deficient aryl groups to optimize interactions with anions. Notably,

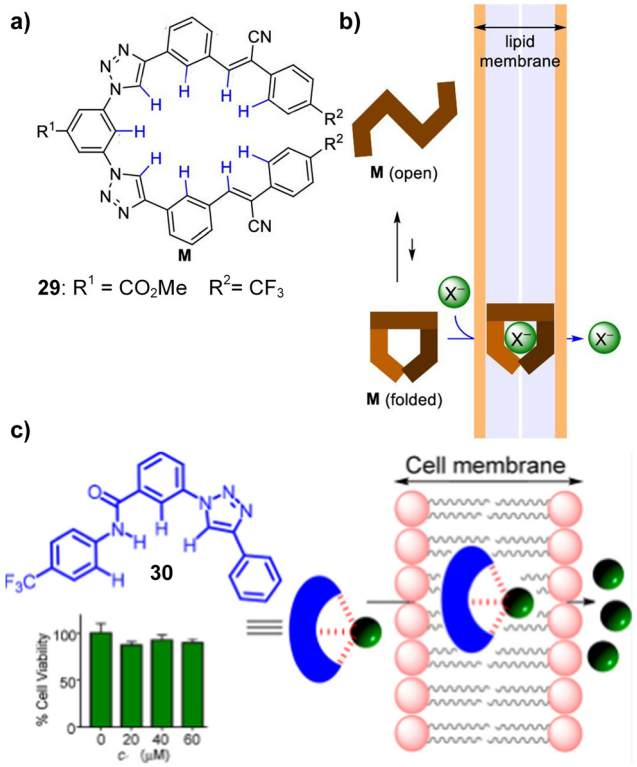

Fig. 20 (a) Chemical structure of **29**. (b) Schematic representation of conformational change and transmembrane anion transport of **29**. (c) Chemical structure of **30**, cell viability assay toward MCF7 cells at variable concentrations of **30** for 24 h and anion transport diagram for **30**. Reproduced with permission from ref. 108 (Copyright 2022 The American Chemical Society) and ref. 109 (Copyright 2022 The American Chemical Society).

29, due to its helical conformation, exhibits high selectivity and transport efficiency for chloride ions relative to other monovalent anions. This effect is attributed to the higher charge density of chloride ions, which allows them to form more stable H-bonds with the receptor through strong dipole–ion interactions of the C–H groups. This not only highlights the role of precise molecular design in regulating ion recognition and selectivity but also demonstrates how molecular control can optimize transmembrane transport performance (Fig. 20(b)).

Talukdar *et al.* further derivatized the triazol foldamer system by designing a structurally much simpler **30** through introducing an electron-withdrawing CF_3 group, causing a push–pull effect (Fig. 20(c)).[109] Among the group of similar molecules tested, **30** shows the highest anion transport activity in model membrane, demonstrating excellent chloride ion transport efficiency. At the cellular level, experiments using the chloride-sensitive dye MQAE confirm that **30** can effectively transport chloride ions into cells, and MTT assays indicate that **30** is non-toxic to cells.

4. Differential repulsive forces-induced helical foldamers as ion transporters

With a proper separation distance, repulsive forces between N-atoms are generally larger than those between N-atoms and O-atoms. Based on this principle, in 2016, Dong *et al.* introduced a new type of biomimetic transmembrane channel, constructed from helically folded macromolecules by taking advantage of differential repulsive forces among heteroatoms (Fig. 21(a) and (b)).[110] The average lengths of channels **31a** and **31b** are 3.3 nm and 1.4 nm respectively, with an estimated pore size of about 0.55 nm (Fig. 21(c)). Fluorescence microscopy imaging and fluorescence titration experiments show that **31a** exists in lipid membranes as a single helix, with its length sufficient to span the entire hydrophobic region. Single-channel electrophysiological experiments demonstrate the channel formed from both **31a** and **31b** within phospholipid bilayers. Notably, **31a**, owing to its longer length and single-molecule channel properties, exhibits higher stability and a longer channel lifespan compared to the shorter **31b** (Fig. 21(d) and (e)). The experimental results indicate that channels **31a** and **31b** possess efficient selective transport capabilities for protons and cations, with their transport activity surpassing that of the naturally occurring peptide antibiotic channel gA and selectivity following Eisenman sequence III.[111] Exhibiting intriguing transport-related properties, these helical macromolecular channels hold good potential for creating artificial transmembrane channels and nanoporous materials, which

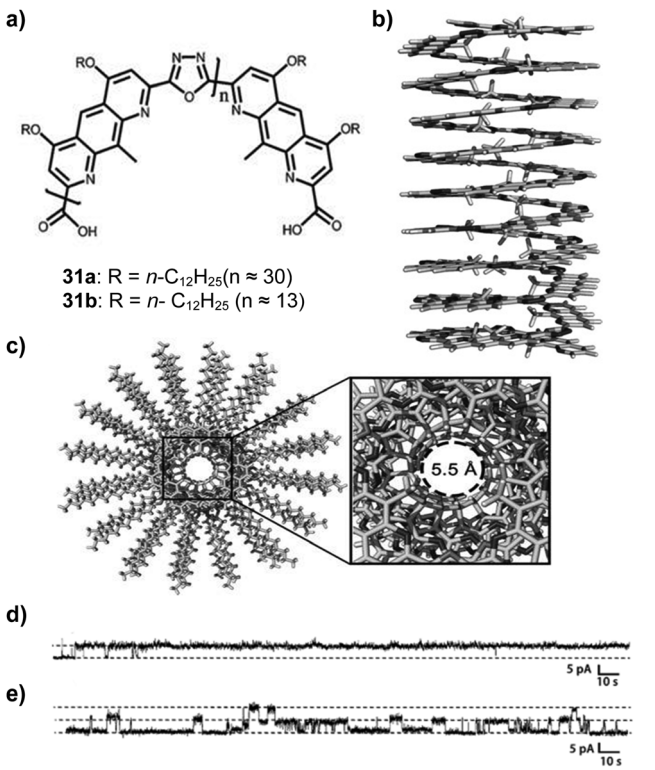

Fig. 21 (a) Molecular design of foldamers **31**. (b) – (c) Conformational model of helical macromolecule **31a** obtained using the COMPASS force field. The pore size is estimated to be about 0.55 nm. Planar lipid bilayer experiments of the helix channel. Electrophysiology channel recordings of (d) **31a** and (e) **31b** in symmetrical baths filled with 0.5 M KCl solution at 150 mV. Reproduced with permission from ref. 110 (Copyright 2016 Wiley).

may show remarkable stability and efficient ion transport capabilities.

Expanding upon their previous work, Dong *et al.* designed another class of artificial ion channel based on a helical polymer backbone, uniquely distinguished by the covalent modification of multiple quaternary ammonium groups on the inner surface of channel **32** for achieving efficient exclusion of alkali metal ions (Fig. 22(a)).[112] The research team successfully grafted multiple positively charged quaternary ammonium groups onto the surface of the helical polymer cavity. This modification not only preserves the intrinsic structure of the helical polymer but also imparts new functional properties to **32**. Specifically, the presence of these positively charged groups leads to high selectivity for anions (*e.g.*, Cl^- ions) while virtually eliminating cations (*e.g.*, alkali metal ions) because of electrostatic repulsion between the cations and the positive charges within the channel. In addition, the molecular design of **32** somewhat mimics the size exclusion and electrostatic repulsion mechanisms of natural protein channels, giving rise to high ionic selectivity. Experimental data show that **32** has a Cl^-/Na^+ selectivity ratio of 41, indicating exceptionally high efficiency in transporting chloride ions than sodium ions (Fig. 22(b)). This finding is of great importance for understanding and simulating the selective transport mechanisms of natural protein channels.

By paring triazole groups with pyridine groups, Liu's group reported an artificial potassium channel **33** constructed through helical stacking (Fig. 23(a) and (b)).[113] Self-assembled channel **33** displays an exceptionally high K^+/Na^+ selectivity. Further utilizing this pair of structural motifs, Zeng *et al.* prepared the polymer-based channel **34** such as $\mathbf{P_{17}}$, endowed with an array of distinctive cation-binding electron-rich heteroatoms (Fig. 23(c)).[114] Nanotubes $\mathbf{P_{23}}$ and $\mathbf{P_{27}}$ averaging 2.3 and 2.7 nm in length were successfully made and were found to mediate highly efficient transport of K^+ ions as a consequence of hydrophilic electron-rich hollow cavities that are 3 Å in diameter and that matches diameter of K^+ ion (2.76 Å). And exceptionally high K^+ and Na^+ selectivity values of 16.3 (Fig. 23(e)) and 12.6, respectively, were achieved, a notably

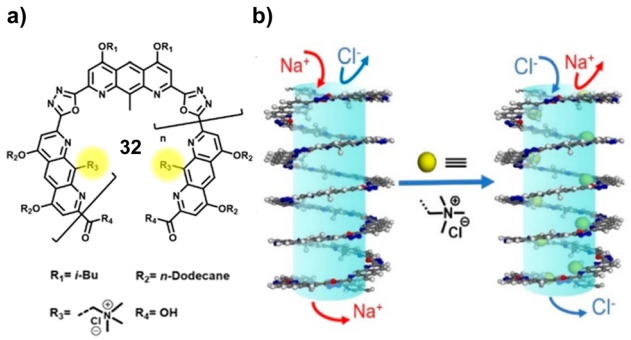

Fig. 22 (a) Chemical structure of **32**. (b) Schematic illustration of the forces behind the Cl^--transporting and cation-rejecting capacity of **32**. Reproduced with permission from ref. 112 (Copyright 2020 The American Chemical Society).

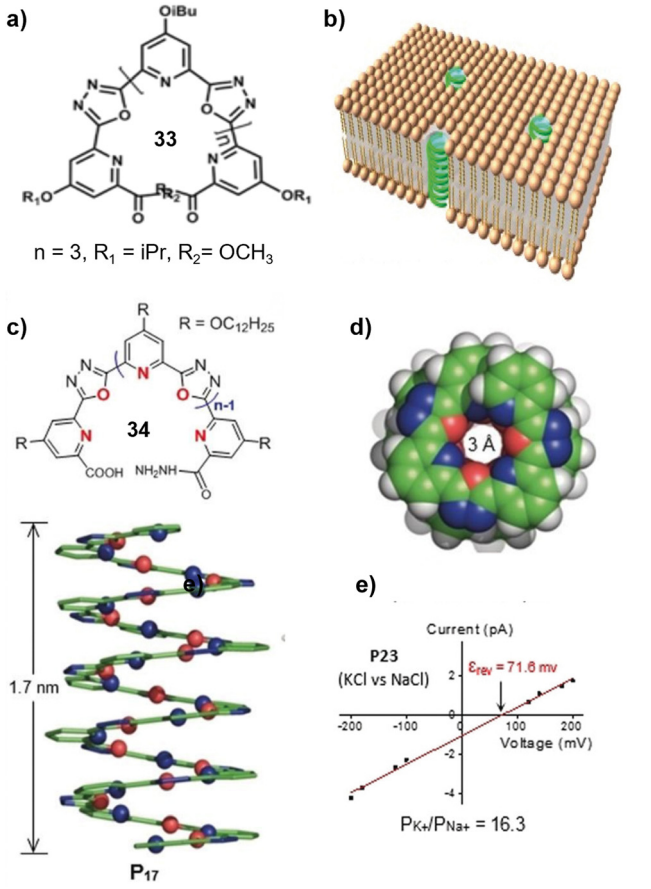

Fig. 23 (a) Chemical structure of **33**. (b) Self-assembled **33** functioning in the lipid bilayer membrane. (c) Molecular design of polymeric channels **34** as represented by $\mathbf{P_{17}}$ that contains an average of 17 repeating units computationally determined at the wB97X/6-31G* level. (d) Top view of computationally optimized helical structural of $\mathbf{P_{17}}$, showing a hollow cavity of 3 Å in diameter. (e) The linear relationship of current traces *versus* voltages for $\mathbf{P_{23}}$ in the planar lipid bilayer, yielding a K^+/Na^+ selectivity of 16.3. Reproduced with permission from ref. 113 (Copyright 2017 Wiley) and ref. 114 (Copyright 2020 Wiley).

significant achievement. Further studies indicate that the correlation between the length of the channels and the hydrophobic thickness of the lipid bilayer may be pivotal in determining the rate and selectivity of ion transport by $\mathbf{P_{23}}$ and $\mathbf{P_{27}}$, emphasizing the dynamic adaptability and capacity of these channels to accommodate larger ions.

By harnessing the structural merits of aromatic helical backbone **33** and employing a sequence substitution strategy involving replacing some or all pyridine units with 1,10-phenanthroline motifs, Dong *et al.* created oligomers **35b** and **35c**. These oligomers show a similar capacity to self-assemble into channels, generating a lumen size varying from 3.8 to 2.3 Å and exhibiting excellent ion selectivity and transport activity through manipulation of cavity size (Fig. 24).[115] In terms of K^+ transport rate derived from vesicle-base assays, **35b** is 8 times as fast as **35c** that in turn is 10 times faster than **35a**. In terms of transport selectivity, **35a** and **35b** show concentration-dependent K^+/Na^+ selectivity factors of up to 22.7 and 32.6,

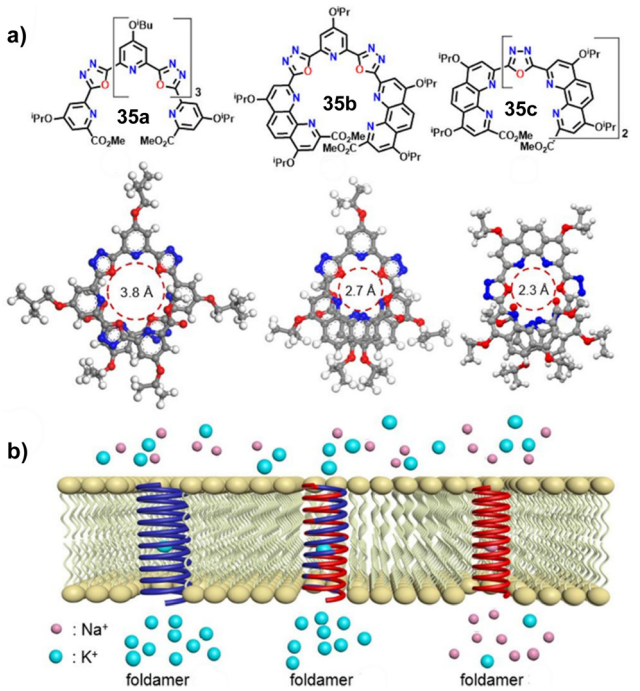

Fig. 24 (a) Chemical structures of **35**. (b) Schematic representation of ion channels formed by self-assembly of **35**. Reproduced with permission from ref. 115 (Copyright 2021 The American Chemical Society).

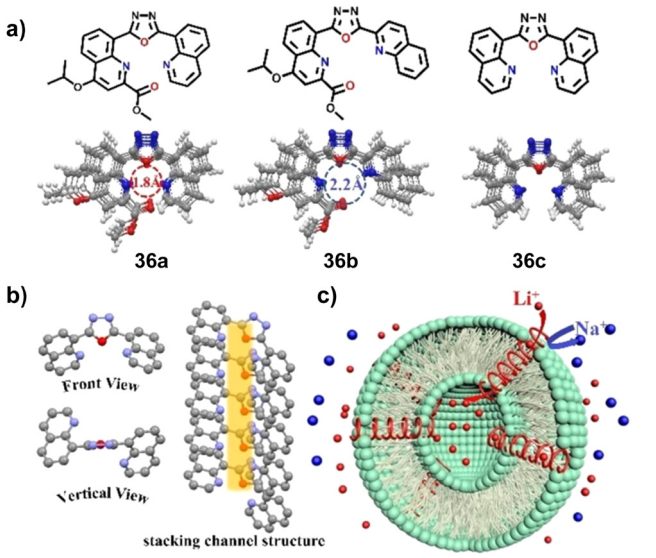

Fig. 25 (a) Chemical structure of **36**. (b) Single crystal structure of **36c** and its linearly self-assembling channel structure. (c) Cartoon of transmembrane transport of supramolecular Li^+ channels. Reproduced with permission from ref. 116 (Copyright 2023 Wiley).

respectively, while **35c** interestingly displays Na^+/K^+ selectivity factors of up to 5.2. It is worth pointing out that all these selectivity values were determined using LUVs and therefore are not very accurate particularly when compared to the selectivity values determined using single channel current traces.

By additionally replacing pyridine units with quinoline motifs, Dong's group developed a class of artificial lithium channel **36a** and **36b**, transporting lithium ions through electron-rich narrow-sized pores adjustable in both size and cation-binding heteroatoms (Fig. 25(a)).[116] Hill analyses of the vesicle-based kinetic data give EC_{50} (Li^+) values of 1.52 μM (1.61 mol% relative to lipid) for **36a**, 0.88 μM (0.93 mol %) for **36b** and no detectable activity for **36c**, respectively. These observations may indicate that four coordination sites as found in **36a** and **36b** are the basic requirement for ion transport. Based on the single channel current traces, **36a** achieves a lithium conductance rate of 27.1 pS. Selectivitywise, while **36a** exhibits concentration-dependent high Li^+/Na^+ transport selectivity from 15.1 to 23.0, Li^+/Na^+ transport selectivity of **36b** was determined to be up to 1.3. Again, do note that these values were determined using LUVs, only providing a qualitative estimate of the ion transport selectivity. Further study shows that **36a** displays minimal transport of Na^+, K^+, Mg^{2+} and Ca^{2+} ions.

In 2024, Dong *et al.* carried out some minor structural modifications of **36**, generating channels **37** of 2.1 Å in diameter (Fig. 26).[117] In essence, **37** mimics the intricate pentahydrate binding motif of sodium ions to good extent (Fig. 26(a)), achieving efficient transmembrane sodium ion permeation

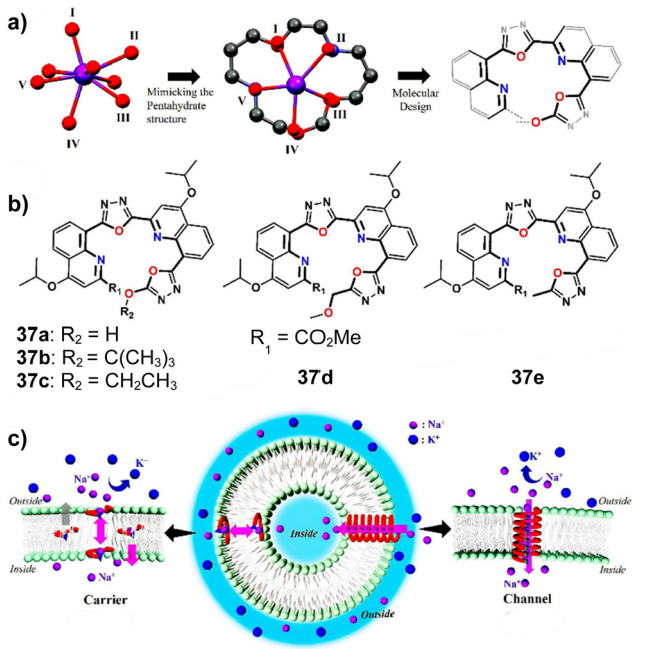

Fig. 26 (a) Crystal structure of octahydrate sodium ion as well as the rational design of helically folded nanopores finely replicating the pentahydrate structure of sodium ion. (b) Chemical structures of nanopore-forming molecules **37**. (c) Cartoon of sodium transmembrane permeation through carrier mode (**37a** and **37b**) and channel mode (**37c–37e**). Reproduced with permission from ref. 117 (Copyright 2024 The American Chemical Society).

with significant ion selectivity. Among the channels studied, **37a** is the most Na^+-selective, demonstrating a LUV-based Na^+/K^+ ion selectivity factor 20.4. It is particularly noteworthy that

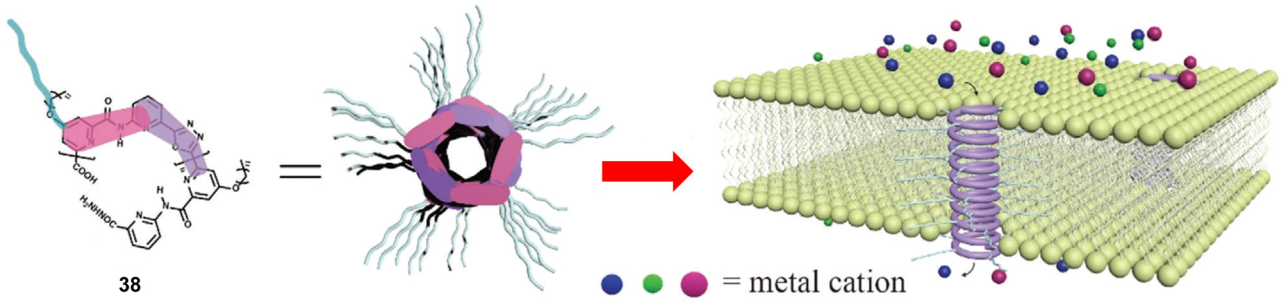

Fig. 27 Helical polymer nanochannel **38** inserting into the lipid bilayer membrane. Reproduced with permission from ref. 118 (Copyright 2020 Wiley).

minor structural changes in the nanopore could lead to changes in ion transport mechanism, *e.g.*, from channel to carrier mechanisms. Their data reveal that the channel mechanism dominates over the carrier mechanism (Fig. 26(c)). Additionally, this work suggests the spatial position and number of coordination sites within the nanopore to be very crucial for sodium ion selectivity.

5. Hybrid helical foldamers as ion transporters

Combing repulsive forces with intramolecular H-bonds to drive the molecular chain to fold in a specific direction, Dong *et al.* developed a self-assembled helically folded nanochannels through introduction of aromatic amide and pyridine-oxadiazole structural motifs into the same molecular backbone (Fig. 27).[118] Helical channel **38** exhibits significant activity in transmembrane transport, especially in transporting alkali metal ions, albeit with relatively weak selectivity in the decreasing order of $Cs^+ > Rb^+ > K^+ \approx Na^+ > Li^+$. Very significantly, the conductance rate of **38**, as measured utilizing single channel current traces, reaches an impressive value of 50.1 pS, surpassing the 39 pS recorded for the natural channel gA under comparable conditions.[110] This underscores the potential to design channels with specific properties through chemical alterations of the helical structural sequence, thereby offering new possibilities for the functional design of nanochannels.

By combining with coordination bond, Liu *et al.* reported a pioneering ligand-gated ion channel, a unique switching mechanism that was achieved through the ion coordination-induced transformation between a hollow single helix and an intertwined double helix (Fig. 28).[119] Employing a carefully designed aromatic helical trimer molecule **39**, the research team achieves reversible control of ion channel activity within lipid bilayers by adding and removing Cu^+ ions (Fig. 28(d)). In the absence of Cu^+ ions, **39** spontaneously assembles into one-dimensional hollow helical tubes through π–π interactions, enabling their embedding into lipid bilayers to form stable ion channels. Dynamic adjustment of its internal cavity can then take place through chemical stimuli. That is, upon adding Cu^+ ions, both triazole and phenanthroline units in **39** can form coordination bonds with Cu^+ ions. This triggers the rotation of the triazole units, subsequently converting helically

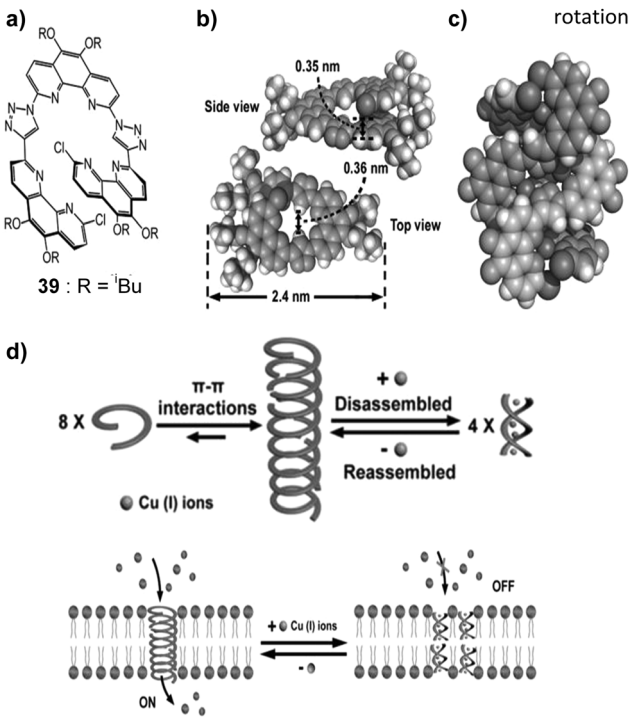

Fig. 28 (a) Chemical structure of **39** and (b) its crystal structure. (c) Crystal structure of $\mathbf{39}_2$-$[Cu(CH_3CN)_4PF_6]_4$. (d) Schematic representation of the tentative formation, disassembly and reassembly of the 1D hollow helical tubes from **39**. (e) Schematic representation of the reversible ligand-gated ion channel formed by **39** triggered by Cu^+ and $NH_3{\cdot}H_2O$. Reproduced with permission from ref. 119 (Copyright 2020 Wiley).

stacked **39** into an intertwined double helix structure (Fig. 28(d)). By using $NH_3{\cdot}H_2O$ as a chelating agent to compete with **39** in binding Cu^+ ions, the double helix structure can be dissociated, reverting to the single helix structure and restoring its channel function (Fig. 28(e)). This structural transition between single and double helices not only showcases precise regulatory capabilities at the molecular level but also has significant application potential in materials science and nanotechnology.

6. Conclusions and outlooks

In this review, we have conducted a comprehensive analysis of artificial transmembrane transporters derived from aromatic

foldamers, outlining key scientific achievements and innovations in this emerging field. The design of these transporters sometimes mirrors those of natural ion channels and aquaporin proteins, presenting new strategies for precisely manipulating transmembrane ion transport and intelligent material design.

One of the greatest advantages of these aromatic foldamers rigidified by intramolecular H-bonds or differential repulsive forces lies in their exceptional molecular design flexibility. The strategic utilization of helical and macrocyclic structures in the field of aromatic foldamers is crucial for regulating transport of ions, water and protons across lipid bilayers, emphasizing the importance of meticulous molecular design in achieving specific functionalities. Significant progresses have been made in creating highly selective ion channels for K^+, H^+ and Li^+ as well as salt- and even proton-rejecting water channels, with progress in achieving high Na^+ selectivity lagging far behind. And these foldamer-derived transporters have shown potential beyond academic research, extending into therapeutic realms including anticancer treatment and managing channel-associated diseases like cystic fibrosis, Bartter Syndromes and Liddle's Syndrome. They also may enable customization for specific biomedical applications such as drug delivery, sensor development and antimicrobial agent design. Furthermore, their possible applications in water treatment, seawater desalination, and as components of biomimetic membranes underscore their adaptability to various technological demands.

These exciting advances have not only deepened our comprehension of membrane transport mechanisms but also help to pave the way for the development of new therapeutic approaches and efficient biotechnological applications to great extent. With the continuous advancement of chemical tools, synthetic biology and materials science, we anticipate that this field will witness further breakthroughs, which will have profound implications for health, the environment, and industry. While we keenly await the innovative solutions that aromatic foldamers may offer to global challenges in the future, it is important to acknowledge that they still confront several challenges in both fundamental and applied settings.

The foremost challenge concerns attaining or even surpassing the exceptional transport selectivity displayed by natural channel proteins as majority of artificial versions falls significantly short in this regard. Secondly, the connection between the structure and function of many artificial transporters is still not fully understood, and their operational duration needs further improvement. Third, most artificial ion channels exhibit non-specific cytotoxicity, affecting both cancerous and healthy cells, which limits their potential for drug development. Therefore, there is a pressing need for the installation of gating mechanisms that respond to external stimuli like chemicals, electricity, light, or temperature changes. Lastly, efficient synthesis and precise structure-based functional design of these aromatic foldamers remain technical bottlenecks, calling for innovative solutions while necessitating further in-depth research and collaboration.

Addressing these challenges is crucial for advancing scientific research and requires innovative structural designs to expand the applicability of foldamer-derived artificial transporters. To propel this field forward, in addition to more intelligent design of molecular structures and functions, future research efforts could prioritize on (1) utilizing computational chemistry and molecular dynamics simulations to guide the design of helical or macrocyclic aromatic foldamers, enhancing ion selectivity and transport efficiency while providing deeper insights into transport mechanisms, (2) conducting both *in vitro* and *in vivo* experiments to assess the biocompatibility and potential toxicity of aromatic foldamers, along with detailed analyses of metabolic pathways, to ensure their safety as drug delivery systems and promote their application in clinical and environmental settings, (3) interdisciplinary collaborations across chemistry, biology, materials science, and pharmacology to expedite knowledge exchange and technological integration, collectively advancing the design and applications of aromatic foldamers in diverse fields, (4) incorporating green chemistry principles into synthesis strategies by exploring renewable resources, using environmentally friendly solvents, reducing the reliance on harmful solvents, and enhancing synthetic efficiency and sustainability, and (5) integrating these transporters into more complex systems, such as embedding aromatic foldamers into functional biomimetic membranes and smart materials, enabling responsiveness and regulation in response to environmental stimuli for separation and other applications.

Author contributions

D. Z. wrote the review, W. C., J. S. and Zeng wrote and edited the review.

Data availability

No primary research results, software or code have been included and no new data were generated or analysed as part of this review.

Conflicts of interest

There are no conflicts to declare.

Acknowledgements

This work is supported by the National Natural Science Foundation of China (No. 22271049 and NO. 22371048), the Natural Science Foundation of Fujian Province (No. 2023J01054) and a start-up grant from Fuzhou University.

Notes and references

1 L. Movileanu, *J. Biochem. Biophys. Methods*, 1999, **38**, 209.
2 E. A. Seyfarth, *Biol. Cybern.*, 2006, **94**, 2.

3 D. J. Hill, M. J. Mio, R. B. Prince, T. S. Hughes and J. S. Moore, *Chem. Rev.*, 2001, **101**, 3893.
4 D. A. Doyle, J. M. Cabral, R. A. Pfuetzner, A. Kuo, J. M. Gulbis, S. L. Cohen, B. T. Chait and R. MacKinnon, *Science*, 1998, **280**, 69.
5 J. H. Morais-Cabral, Y. Zhou and R. MacKinnon, *Nature*, 2001, **414**, 37.
6 W. A. Catterall, *J. Physiol.*, 2012, **590**, 2577.
7 J. Payandeh, T. Scheuer, N. Zheng and W. A. Catterall, *Nature*, 2011, **475**, 353.
8 M. Hans, S. Luvisetto, M. E. Williams, M. Spagnolo, A. Urrutia, A. Tottene, P. F. Brust, E. C. Johnson, M. M. Harpold, K. A. Stauderman and D. Pietrobon, *J. Neurosci.*, 1999, **19**, 1610.
9 X. Hou, L. Pedi, M. M. Diver and S. B. Long, *Science*, 2012, **338**, 1308.
10 T. J. Jentsch, V. Stein, F. Weinreich and A. A. Zdebik, *Physiol. Rev.*, 2002, **82**, 503.
11 G. Blanco and R. W. Mercer, *Am. J. Physiol.*, 1998, **275**, F633.
12 E. E. Strehler, *Biochem. Biophys. Res. Commun.*, 2015, **460**, 26.
13 C. J. Pedersen, *J. Am. Chem. Soc.*, 1967, **89**, 7017.
14 B. C. Pressman, E. J. Harris, W. S. Jagger and J. H. Johnson, *Proc. Natl. Acad. Sci. U. S. A.*, 1967, **58**, 1949.
15 I. Tabushi, Y. Kuroda and K. Yokota, *Tetrahedron Lett.*, 1982, **23**, 4601.
16 A. Nakano, Q. Xie, J. V. Mallen, L. Echegoyen and G. W. Gokel, *J. Am. Chem. Soc.*, 1990, **112**, 1287.
17 M. R. Ghadiri, J. R. Granja, R. A. Milligan, D. E. McRee and N. Khazanovich, *Nature*, 1993, **366**, 324.
18 M. R. Ghadiri, J. R. Granja and L. K. Buehler, *Nature*, 1994, **369**, 301.
19 B. Baumeister, N. Sakai and S. Matile, *Angew. Chem., Int. Ed.*, 2000, **39**, 1955.
20 N. Sakai, J. Mareda and S. Matile, *Acc. Chem. Res.*, 2008, **41**, 1354.
21 G. Das, P. Talukdar and S. Matile, *Science*, 2002, **298**, 1600.
22 A. Vargas Jentzsch, A. Hennig, J. Mareda and S. Matile, *Acc. Chem. Res.*, 2013, **46**, 2791.
23 J. T. Davis, P. A. Gale and R. Quesada, *Chem. Soc. Rev.*, 2020, **49**, 6056.
24 X. Wu, A. M. Gilchrist and P. A. Gale, *Chem*, 2020, **6**, 1296.
25 J. Yang, G. Yu, J. L. Sessler, I. Shin, P. A. Gale and F. Huang, *Chem*, 2021, **7**, 3256.
26 A. Mondal, M. Ahmad, D. Mondal and P. Talukdar, *Chem. Commun.*, 2023, **59**, 1917.
27 J. de Jong, J. E. Bos and S. J. Wezenberg, *Chem. Rev.*, 2023, **123**, 8530.
28 M. Ahmad, S. A. Gartland and M. J. Langton, *Angew. Chem., Int. Ed.*, 2023, **62**, e202308842.
29 R. Cao, R. B. Rossdeutcher, Y. Zhong, Y. Shen, D. P. Miller, T. A. Sobiech, X. Wu, L. S. Buitrago, K. Ramcharan, M. I. Gutay, M. F. Figueira, P. Luthra, E. Zurek, T. Szyperski, B. Button, Z. Shao and B. Gong, *Nat. Chem.*, 2023, **15**, 1559.
30 H. Gill, M. R. Gokel, M. McKeever, S. Negin, M. B. Patel, S. Yin and G. W. Gokel, *Coord. Chem. Rev.*, 2020, **412**, 213264.
31 S.-P. Zheng, L.-B. Huang, Z. Sun and M. Barboiu, *Angew. Chem., Int. Ed.*, 2021, **60**, 566.
32 T. Yan, X. Zheng, S. Liu, Y. Zou and J. Liu, *Sci. China: Chem.*, 2022, **65**, 1265.
33 X. Y. Yuan, J. Shen and H. Q. Zeng, *Chem. Commun.*, 2024, **60**, 482.
34 J. Shen, C. L. Ren and H. Q. Zeng, *Acc. Chem. Res.*, 2022, **55**, 1148.
35 Y. P. Huo and H. Q. Zeng, *Acc. Chem. Res.*, 2016, **49**, 922.
36 B. Gong, *Faraday Discuss.*, 2018, **209**, 415.
37 W. Song and M. Kumar, *Curr. Opin. Chem. Eng.*, 2019, **25**, 9.
38 I. Kocsis, Z. Sun, Y. M. Legrand and M. Barboiu, *npj Clean Water*, 2018, **1**, 13.
39 M. Di Vincenzo, A. Tiraferri, V.-E. Musteata, S. Chisca, R. Sougrat, L.-B. Huang, S. P. Nunes and M. Barboiu, *Nat. Nanotechnol.*, 2021, **16**, 190.
40 A. Roy, J. Shen, H. Joshi, W. Song, Y.-M. Tu, R. Chowdhury, R. Ye, N. Li, C. Ren, M. Kumar, A. Aksimentiev and H. Q. Zeng, *Nat. Nanotechnol.*, 2021, **16**, 911.
41 S. H. Gellman, *Acc. Chem. Res.*, 1998, **31**, 173.
42 J. Applequist and J. D. Glickson, *J. Am. Chem. Soc.*, 1971, **93**, 3276.
43 M. Narita, M. Doi, K. Kudo and Y. Terauchi, *Bull. Chem. Soc. Jpn.*, 1986, **59**, 3553.
44 J. Bella, C. Aleman, J. M. Fernandez-Santin, C. Alegre and J. A. Subirana, *Macromolecules*, 1992, **25**, 5225.
45 F. López-Carrasquero, C. Alemán and S. Muñoz-Guerra, *Biopolymers*, 1995, **36**, 263.
46 V. E. Schmidt, *Angew. Makromol. Chem.*, 1970, **14**, 185.
47 F. Chen, G. Lepore and M. Goodman, *Macromolecules*, 1974, **7**, 779.
48 K. A. Bode and J. Applequist, *Macromolecules*, 1997, **30**, 2144.
49 R. P. Cheng, S. H. Gellman and W. F. DeGrado, *Chem. Rev.*, 2001, **101**, 3219.
50 P. Sang and J. F. Cai, *Chem. Soc. Rev.*, 2023, **52**, 4843.
51 P. S. Shirude, E. R. Gillies, S. Ladame, F. Godde, K. Shin-ya, I. Huc and S. Balasubramanian, *J. Am. Chem. Soc.*, 2007, **129**, 11890.
52 B. Gong, *Acc. Chem. Res.*, 2008, **41**, 1376.
53 D.-W. Zhang, X. Zhao, J.-L. Hou and Z.-T. Li, *Chem. Rev.*, 2012, **112**, 5271.
54 Y. Hamuro, S. J. Geib and A. D. Hamilton, *Angew. Chem., Int. Ed. Engl.*, 1994, **33**, 446.
55 J. C. Nelson, J. G. Saven, J. S. Moore and P. G. Wolynes, *Science*, 1997, **277**, 1793.
56 V. Berl, I. Huc, R. G. Khoury, M. J. Krische and J.-M. Lehn, *Nature*, 2000, **407**, 720.
57 D. M. Bassani, J.-M. Lehn, G. Baum and D. Fenske, *Angew. Chem., Int. Ed. Engl.*, 1997, **36**, 1845.
58 J. Zhu, R. D. Parra, H. Q. Zeng, E. Skrzypczak-Jankun, X. C. Zeng and B. Gong, *J. Am. Chem. Soc.*, 2000, **122**, 4219.
59 B. Gong, H. Q. Zeng, J. Zhu, L. Yua, Y. Han, S. Cheng, M. Furukawa, R. D. Parra, A. Y. Kovalevsky, J. L. Mills, E. Skrzypczak-Jankun, S. Martinovic, R. D. Smith, C. Zheng, T. Szyperski and X. C. Zeng, *Proc. Natl. Acad. Sci. U. S. A.*, 2002, **99**, 11583.
60 I. Saraogi and A. D. Hamilton, *Chem. Soc. Rev.*, 2009, **38**, 1726.
61 Z.-T. Li, J.-L. Hou and C. Li, *Acc. Chem. Res.*, 2008, **41**, 1343.
62 G. Guichard and I. Huc, *Chem. Commun.*, 2011, **47**, 5933.
63 H. L. Fu, Y. Liu and H. Q. Zeng, *Chem. Commun.*, 2013, **49**, 4127.
64 W. Q. Ong and H. Q. Zeng, *J. Inclusion Phenom. Macrocyclic Chem.*, 2013, **76**, 1.
65 B. Gong and Z. Shao, *Acc. Chem. Res.*, 2013, **46**, 2856.
66 Y. Ferrand and I. Huc, *Acc. Chem. Res.*, 2018, **51**, 970.
67 E. A. John, C. J. Massena and O. B. Berryman, *Chem. Rev.*, 2020, **120**, 2759.
68 V. Koehler, A. Roy, I. Huc and Y. Ferrand, *Acc. Chem. Res.*, 2022, **55**, 1074.
69 J.-Y. Chen and J.-L. Hou, *Org. Chem. Front.*, 2018, **5**, 1728.
70 D.-W. Zhang, H. Wang and Z.-T. Li, *Macromol. Rapid Commun.*, 2017, **38**, 1700179.
71 A. J. Helsel, A. L. Brown, K. Yamato, W. Feng, L. Yuan, A. J. Clements, S. V. Harding, G. Szabo, Z. Shao and B. Gong, *J. Am. Chem. Soc.*, 2008, **130**, 15784.
72 L. Yuan, W. Feng, K. Yamato, A. R. Sanford, D. Xu, H. Guo and B. Gong, *J. Am. Chem. Soc.*, 2004, **126**, 11120.
73 A. R. Sanford, L. Yuan, W. Feng, K. Yamato, R. A. Flowers and B. Gong, *Chem. Commun.*, 2005, 4720.
74 M. A. Kline, X. Wei, I. J. Horner, R. Liu, S. Chen, S. Chen, K. Y. Yung, K. Yamato, Z. Cai, F. V. Bright, X. C. Zeng and B. Gong, *Chem. Sci.*, 2015, **6**, 152.
75 X. Wei, G. Zhang, Y. Shen, Y. Zhong, R. Liu, N. Yang, F. Y. Almkhaizim, M. A. Kline, L. He, M. Li, Z.-L. Lu, Z. Shao and B. Gong, *J. Am. Chem. Soc.*, 2016, **138**, 2749.
76 Y. Shen, F. Fei, Y. L. Zhong, C. H. Fan, J. L. Sun, J. Hu, B. Gong, D. M. Czajkowsky and Z. Shao, *ACS Cent. Sci.*, 2021, **7**, 2092.
77 P. Y. Xin, S. Tan, Y. D. Wang, Y. H. Sun, Y. Wang, Y. Q. Xu and C.-P. Chen, *Chem. Commun.*, 2017, **53**, 625.
78 P. Y. Xin, S. Tan, Y. H. Sun, Q. Ren, W. P. Dong, J. J. Guo, T. Jiang and C.-P. Chen, *Chem. Commun.*, 2017, **53**, 5322.
79 H. Behera and N. Madhavan, *J. Am. Chem. Soc.*, 2017, **139**, 12919.
80 H. Behera, V. Ramkumar and N. Madhavan, *Org. Biomol. Chem.*, 2017, **15**, 4937.
81 P. Saha and N. Madhavan, *Org. Lett.*, 2020, **22**, 5104.
82 R. Cao, R. B. Rossdeutcher, Y. Zhong, Y. Shen, D. P. Miller, T. A. Sobiech, X. Wu, L. S. Buitrago, K. Ramcharan, M. I. Gutay, M. F. Figueira, P. Luthra, E. Zurek, T. Szyperski, B. Button, Z. Shao and B. Gong, *Nat. Chem.*, 2023, **15**, 1559.
83 A. V. Jentzsch, D. Emery, J. Mareda, S. K. Nayak, P. Metrangolo, G. Resnati, N. Sakai and S. Matile, *Nat. Commun.*, 2012, **3**, 905.

84 G. Y. Rychkov, M. Pusch, M. L. Roberts, T. J. Jentsch and A. H. Bretag, *J. Gen. Physiol.*, 1998, **111**, 653.
85 X. Zhou, G. Liu, K. Yamato, Y. Shen, R. Cheng, X. Wei, W. Bai, Y. Gao, H. Li, Y. Liu, F. Liu, D. M. Czajkowsky, J. Wang, M. J. Dabney, Z. Cai, J. Hu, F. V. Bright, L. He, X. C. Zeng, Z. Shao and B. Gong, *Nat. Commun.*, 2012, **3**, 949.
86 C.-Y. Wu, S. Su, X. Zhang, R. Liu, B. Gong and Z.-L. Lu, *Angew. Chem., Int. Ed.*, 2023, **62**, e202303242.
87 V. Vijayvergiya, R. Wilson, A. Chorak, P. F. Gao, T. A. Cross and D. D. Busath, *Biophys. J.*, 2004, **87**, 1697.
88 M. L. Zeidel, S. V. Ambudkar, B. L. Smith and P. Agre, *Biochemistry*, 1992, **31**, 7436.
89 W. Q. Ong, H. Q. Zhao, Z. Y. Du, J. Z. Y. Yeh, C. L. Ren, L. Z. W. Tan, K. Zhang and H. Q. Zeng, *Chem. Commun.*, 2011, **47**, 6416.
90 W. Q. Ong, H. Q. Zhao, X. Fang, S. Woen, F. Zhou, W. Yap, H. B. Su, S. F. Y. Li and H. Q. Zeng, *Org. Lett.*, 2011, **13**, 3194.
91 H. Q. Zhao, W. Q. Ong, F. Zhou, X. Fang, X. Y. Chen, S. F. Y. Li, H. Su, N.-J. Cho and H. Q. Zeng, *Chem. Sci.*, 2012, **3**, 2042.
92 H. Q. Zhao, S. Sheng, Y. H. Hong and H. Q. Zeng, *J. Am. Chem. Soc.*, 2014, **136**, 14270.
93 J. Shen, R. J. Ye, A. Romanies, A. Roy, F. Chen, C. L. Ren, Z. Liu and H. Q. Zeng, *J. Am. Chem. Soc.*, 2020, **142**, 10050.
94 J. Shen, J. R. Fan, R. J. Ye, N. Li, Y. G. Mu and H. Q. Zeng, *Angew. Chem., Int. Ed.*, 2020, **59**, 13328.
95 P. Xin, P. Zhu, P. Su, J.-L. Hou and Z.-T. Li, *J. Am. Chem. Soc.*, 2014, **136**, 13078.
96 A. Roy, H. Joshi, R. J. Ye, J. Shen, F. Chen, A. Aksimentiev and H. Q. Zeng, *Angew. Chem., Int. Ed.*, 2020, **59**, 4806.
97 J. Shen, A. Roy, H. Joshi, L. Samineni, R. J. Ye, Y.-M. Tu, W. Song, M. Skiles, M. Kumar, A. Aksimentiev and H. Q. Zeng, *Nano Lett.*, 2022, **22**, 4831.
98 J. Shen, R. J. Ye, Z. W. Liu and H. Q. Zeng, *Angew. Chem., Int. Ed.*, 2022, **61**, e202200259.
99 N. Agmon, *Chem. Phys. Lett.*, 1995, **244**, 456.
100 J. Shen, D. R, Z. Y. Li, H. Oh, H. Behera, H. Joshi, M. Kumar, A. Aksimentiev and H. Q. Zeng, *Angew. Chem., Int. Ed.*, 2023, **62**, e202305623.
101 T. F. Yan, S. D. Liu, J. Y. Xu, H. C. Sun, S. J. Yu and J. Q. Liu, *Nano Lett.*, 2021, **21**, 10462.
102 H. Jiang, J.-M. Leger and I. Huc, *J. Am. Chem. Soc.*, 2003, **125**, 3448.
103 H. L. Chen, Y. J. Liu, X. B. Cheng, S. B. Fang, Y. L. Sun, Z. Q. Yang, W. Zheng, X. M. Ji and Z. H. Wu, *Angew. Chem., Int. Ed.*, 2021, **60**, 10833.
104 C. Y. Zhang, J. Zhang, W. C. Li, S. Z. Mao and Z. Y. Dong, *ChemPlusChem*, 2021, **86**, 492.
105 Y. R. Choi, M. K. Chae, D. Kim, M. S. Lah and K.-S. Jeong, *Chem. Commun.*, 2012, **48**, 10346.
106 J. H. Lee, J. H. Lee, Y. R. Choi, P. Kang, M.-G. Choi and K.-S. Jeong, *J. Org. Chem.*, 2014, **79**, 6403.
107 J. Shang, W. Si, W. Zhao, Y. Che, J.-L. Hou and H. Jiang, *Org. Lett.*, 2014, **16**, 4008.
108 D. Mondal, M. Ahmad, P. Panwaria, A. Upadhyay and P. Talukdar, *J. Org. Chem.*, 2022, **87**, 10.
109 J. A. Malla, A. Upadhyay, P. Ghosh, D. Mondal, A. Mondal, S. Sharma and P. Talukdar, *Org. Lett.*, 2022, **24**, 4124.
110 C. Lang, W. F. Li, Z. Y. Dong, X. Zhang, F. H. Yang, B. Yang, X. L. Deng, C. Y. Zhang, J. Y. Xu and J. Q. Liu, *Angew. Chem., Int. Ed.*, 2016, **55**, 9723.
111 G. Eisenman and R. Horn, *J. Membr. Biol.*, 1983, **76**, 197.
112 C. Y. Zhang, J. Tian, S. W. Qi, B. Yang and Z. Y. Dong, *Nano Lett.*, 2020, **20**, 3627.
113 C. Lang, X. L. Deng, F. H. Yang, B. Yang, W. Wang, S. W. Qi, X. Zhang, C. Y. Zhang, Z. Y. Dong and J. Q. Liu, *Angew. Chem., Int. Ed.*, 2017, **56**, 12668.
114 F. Chen, J. Shen, N. Li, A. Roy, R. J. Ye, C. L. Ren and H. Q. Zeng, *Angew. Chem., Int. Ed.*, 2020, **59**, 1440.
115 S. W. Qi, C. Y. Zhang, H. Yu, J. Zhang, T. F. Yan, Z. Lin, B. Yang and Z. Y. Dong, *J. Am. Chem. Soc.*, 2021, **143**, 3284.
116 L. Zhang, C. Y. Zhang, X. Dong and Z. Y. Dong, *Angew. Chem., Int. Ed.*, 2023, **62**, e202214194.
117 L. Zhang, J. Tian, Z. Lin and Z. Y. Dong, *J. Am. Chem. Soc.*, 2024, **146**, 8500.
118 S. W. Qi, C. Y. Zhang, T. F. Yan, F. H. Yang, J. Zhang, S. Z. Mao and Z. Y. Dong, *Macromol. Rapid Commun.*, 2020, **41**, 2000099.
119 D. Y. Bai, T. F. Yan, S. Wang, Y. B. Wang, J. Y. Fu, X. M. Fang, J. Y. Zhu and J. Q. Liu, *Angew. Chem., Int. Ed.*, 2020, **59**, 13602.

